Hindawi
Structural Control and Health Monitoring
Volume 2023, Article ID 2857660, 25 pages
https://doi.org/10.1155/2023/2857660

Research Article

Instrumentation of Field-Testing Sites for Dynamic Characterization of the Temperature-Dependent Stiffness of Pavements and Their Layers

Valentin Donev,[1] **Rodrigo Díaz Flores**,[2] **Lukas Eberhardsteiner**,[1] **Luis Zelaya-Lainez**,[2] **Christian Hellmich**,[2] **Martin Buchta**,[3] **and Bernhard L. A. Pichler**[2]

[1]*TU Wien, Institute for Transportation, Karlsplatz 13/230-03, 1040 Vienna, Austria*
[2]*TU Wien, Institute for Mechanics of Materials and Structures, Karlsplatz 13/202, 1040 Vienna, Austria*
[3]*Nievelt Labor GmbH, Betriebsstraße 1, 2011 Höbersdorf, Austria*

Correspondence should be addressed to Valentin Donev; valentin.donev@tuwien.ac.at

Received 14 March 2023; Revised 2 August 2023; Accepted 4 August 2023; Published 28 August 2023

Academic Editor: Fabio Casciati

Falling weight deflectometer (FWD) tests are performed worldwide for assessing the health of pavement structures. Interpretation of FWD-measured surface deflections turns out to be challenging because the behavior of pavement structures is temperature-dependent. In order to investigate the influence of temperature on the overall pavement performance and on the stiffness of individual layers, temperature sensors, asphalt strain gauges, and accelerometers were installed into one rigid (concrete) and two flexible (asphalt) pavement structures, mostly at layer interfaces. Three different methods for installation of the strain gauges are compared. From correspondingly gained experience, it is recommended to install a steel dummy as a place-holder into the surface of hot asphalt layers, immediately after their construction and right before their compaction, and to replace the dummy with the actual sensor right before the installation of the next layer. Concerning the first data obtained from dynamic testing at the field-testing sites, FWD tests performed at different temperatures deliver, as expected, different surface deflections. As for the rigid pavement, sledgehammer strokes onto a metal plate, transmitted to the pavement via a rubber pad, yield accelerometer readings that allow for detection of curling (=temperature-gradient-induced partial loss of contact of the concrete slab from lower layers). In the absence of curling, the here-proposed sledgehammer tests yield accelerometer readings that allow for quantification of the runtime of longitudinal waves through asphalt, cement-stabilized, and unbound layers, such that their stiffness can be quantified using the theory of elastic wave propagation through isotropic media.

1. Introduction

Roads are exposed to variable atmospheric conditions. The corresponding changes in temperature have a significant influence on the performance of rigid and flexible pavement structures:

(1) So-called flexible pavements include layers of asphalt. The stiffness of bituminous asphalt materials decreases with increasing temperature [1, 2].

(2) So-called rigid pavements include concrete slabs. Their temperature-gradient-induced curling (= partial loss of full-face contact along one of the layer interfaces) reduces the structural stiffness of concrete roads [3, 4].

(3) Many pavement structures include unbound granular layers. Their stiffness was shown to be a function of stress level and moisture content. The latter correlates with temperature changes in the unbound layers [5, 6].

Consequently, it is challenging to interpret *different* surface deflections measured during nominally *identical* falling weight deflectometer (FWD) tests performed on *the same* pavement structure at *different* temperatures. The described situation provides the motivation to gain (i) more insights into the load-carrying behavior of multilayered pavement structures subjected to dynamic loading and (ii) direct access to the stiffness of individual layers of interest. To this end, one rigid and two flexible pavement structures are equipped with three types of sensors: (i) Pt100 sensors in order to measure the temperature at specific depths of the pavement structure, (ii) strain gauges in order to quantify the horizontal normal strains of asphalt in radial directions relative to the center of the falling weight during FWD testing, and (iii) accelerometers in order to analyse how dynamic loads propagate through pavement structures.

FWD testing is a worldwide popular nondestructive method for the assessment of the health of pavement structures. FWD tests consist of dropping a standardized weight onto a damped spring system placed over a circular load plate that transmits the dynamic load to the pavement structure. The force history is measured using an integrated load cell. Several displacement sensors measure the vertical deflection history at specific distances from the center of the falling weight [7, 8]. Such sensors include accelerometers, which consist of a mass and spring system and convert the acceleration of the ground into electrical signals [9], geophones, which consist of a coil suspended on a permanent magnet and convert the ground velocity into an electric signal [10], and seismometers, which measure any seismic activity and may convert ground displacement, velocity, or acceleration into electrical signals [8, 11]. Displacement values may be obtained from all types of sensors by integrating the acceleration and velocity signals.

Surface deflections measured during FWD tests are usually evaluated using one of two popular conceptual approaches. The first one refers to the quantification and interpretation of *deflection basin parameters* such as the surface curvature index (SCI) or the AREA parameter, see [7, 12–16]. Similar indexes have been developed for quantification of asymmetric behavior of concrete slabs subjected to central FWD testing [17–19]. The second approach for evaluation of FWD tests refers to back-calculation of properties of the tested pavement structure in order to minimize the difference between measured and simulated deflections. Two types of structural simulation models are frequently used: multilayered elastic half-space models and "dense-liquid" models. The former models explicitly resolve the individual layers of pavement structures [20]. Back-calculation is commonly aimed at quantifying the stiffness of the individual layers. Different commercial programs frequently produce different results even when fed with the same input data [21] because different combinations of layer moduli and thicknesses produce (virtually) the same deflections [8, 22]. The second type of structural models ("dense-liquid models") idealizes pavement structures as an elastic plate resting on a Winkler foundation [23, 24]. Back-calculation is aimed at quantifying the bending stiffness of the plate and the modulus of subgrade reaction of the Winkler foundation. Analytical formulae facilitate the back-calculation procedure, see [3, 25–27]. Notably, back-calculations were also carried out in the context of dynamic analyses with the aid of finite element (FE) simulations [28–31], also with the aim of assessing the influence of longitudinal cracks on FWD test results [32].

The present study builds on experience from FWD research approaches which consisted of equipping road sections and pavement testing facilities with different types of measurement sensors. Common sensors installed for in situ pavement monitoring [33] include horizontal and vertical strain gauges [34, 35], fiber optic sensors [36], LVDTs [37], accelerometers [38], temperature [39], moisture [40], and pressure sensors [41]. They have been proven to be useful in the context of validation of FWD back-calculations [42], in particular to assess the difference between laboratory and back-calculated asphalt moduli [43] and for separating transient and permanent deformations [44]. A variety of strain gauges, pressure cells, deflection, and temperature sensors were installed into flexible pavement, and recommendations were given regarding their selection and use [45]. The readings of embedded strain gauges and pressure cells were compared with back-calculated stresses [46–48] and strains [49–51]. Optical fiber-based sensors were embedded for pavement health monitoring and damage detection [52]. Multidepth deflectometer sensors have been installed to improve the interpretation of FWD data with respect to base and subgrade damage [53]. Moisture and groundwater sensors allowed for assessing the influence of moisture content and depth of the groundwater table on FWD deflections and back-calculated stiffness of the unbound layers [5]. The recorded time history of the deflections measured during an FWD test, together with strain sensor readings, was exploited to study the cross-anisotropic viscoelastic properties of asphalt concrete [54]. MEMS accelerometers have been installed (i) to compute displacement histories either by means of double time-integration or by constrained least-squares estimation and (ii) to compare the resulting data with surface displacements measured by FWD geophones [55].

The present study serves two main purposes: (i) experience with instrumentation of rigid and flexible pavements during their new construction will be gained and shared. This concerns particularly the installation of the strain gauges into asphalt layers. Three different methods will be compared: "method A: cut, install, and cover after asphalt placement," "method B: installation in a fixation tool before asphalt placement," and "method C: use of steel dummy place-holders for the real sensors." (ii) First data from dynamic testing at the innovatively equipped field-testing sites will be presented and discussed. This includes data from both FWD tests and a newly proposed "sledgehammer test." It consists of sledgehammer strokes onto a metal plate, transmitted to the pavement via a rubber pad. The sledgehammer test is performed in order to obtain accelerometer readings that allow for quantification of the runtime of longitudinal waves through asphalt, cement-stabilized, and unbound layers, such that their stiffness can be quantified using the theory of elastic wave propagation through

isotropic media. To this end, acceleration sensors are installed both at the top and the bottom of layers of interest.

The present manuscript is organized as follows. Section 2 describes the three specific field-testing sites together with the corresponding instrumentation layouts. Section 3 refers to the accelerometers: it presents the theoretical foundations for quantification of layer stiffness, the criteria for sensor selection, and the experience gained from the installation of the sensors. Section 4 refers to the asphalt strain gauges: it presents the criteria for sensor selection, three different approaches for the installation of the sensors, and the experience gained with them. Section 5 discusses exemplary data from FWD testing of rigid and flexible pavements, together with results from the sledgehammer tests. Section 6 closes the paper with conclusions drawn from the presented results.

2. Overview of the Three Field-Testing Sites

One rigid and two flexible pavement structures were instrumented to become field-testing sites for FWD experiments. They were equipped with temperature sensors, accelerometers (Section 3), and asphalt strain gauges (Section 4), see Figure 1.

As for temperature measurements, platinum-based detectors with an electrical resistance of 100 Ω, see the Pt100 in Figure 1, were installed in asphalt, concrete, cement-stabilized, and unbound layers. The sensors were connected by means of 4 wires running through Perfluoroalkoxy cables to a LEMO connector. The cables were protected by a Ø5 × 40 mm stainless steel sleeve, a 300 mm heat shrink sleeve, and a waterproof-corrugated plastic tube.

Signals of all installed sensors were recorded during dynamic testing by means of the mobile data acquisition systems DEWE43-A (strain gauges and accelerometers) and KRYPTONi-8 × RTD (temperature sensors) by DEWESoft, see Figure 1. These systems are suitable for measurements at multiple unsheltered field-testing sites because they are water-, dust-, and shockproof, and they are capable of operation within the temperature range from −40°C to 85°C. The required electricity was provided by a portable power bank Novoo 230 Wh, see Figure 1. Between successive measurement days, the connector-ends of all sensor cables were stored inside a stainless steel box near the verge.

Three different types of pavement structures, frequently used on the Austrian motor- and expressways, were instrumented: (i) a rigid pavement consisting of concrete slabs with dowel bars placed along transverse joints and tie bars along longitudinal joints, (ii) a flexible pavement consisting of asphalt concrete layers placed over a cement-stabilized granular layer, and (iii) a flexible pavement consisting of asphalt concrete layers over two unbound granular layers. All three field-testing sites were installed in the course of major rehabilitation treatments.

2.1. Field-Testing Site #1 on Motorway A10. Field-testing site #1 is a concrete slab on the motorway A10, south of Salzburg. A slab of the emergency lane was selected, see Figure 2(a). It has the same pavement structure as the traffic lanes, see Figure 2(c), and it can be closed for FWD measurements without interrupting the traffic. The width and the length of the slab amount to 3.50 m and 5.00 m, respectively, see Figure 2(b). The measurement sensors were installed during the rehabilitation of the motorway. It included the following steps. The existing asphalt and concrete layers were removed such that the subgrade was covered by two unbound granular layers only. The upper unbound granular layer was mixed in-place with cement and water, followed by compaction, in order to transform it into a cement-stabilized layer (L3). A separation layer made of asphalt (L4) was installed. Two concrete layers (L5 and L6) were laid in one pass using a train of two slipform pavers, which are the standard concrete pavement construction techniques in Austria. Both layers are designed according to their function in the pavement structure in order to optimize functional performance (e.g., skid resistance and noise), service life, and costs [56]. This completed new pavement structure is depicted in Figure 2(c).

Sensors were embedded at several depths. Six temperature sensors (T2–T7) were placed at all interfaces between neighboring layers as well as in the middle of the lower concrete layer, see Figure 2(c). Three accelerometers (B2–B4) were installed along a vertical axis running through the central measurement point (MP) for FWD testing, at the interfaces between the subgrade (L1), the unbound layer (L2), the cement-stabilized layer (L3), and the asphalt layer (L4), see Figures 2(b) and 2(c). Four strain gauges (A1–A4) were installed at the bottom of the asphalt layer, see Figure 2(d) for the symmetric crosswise arrangement relative to the measuring point.

Regarding the sequence of sensor installation, sensors B2 and T2 were put in place before the cement-stabilization of L3. Immediately after the stabilization, a trench was cut with an excavator down to the interface between layers L2 and L3. There, the sensors B3 and T3 were installed, the trench was refilled with the excavation material, and the layer was compacted. These works were completed before the start of the main phase of the cement hardening process. Sensors B4 and T4 were installed shortly before the placement of the asphalt concrete. The strain gauges and the temperature sensors T5, T6, and T7 were installed immediately after the construction of the asphalt layer and the lower concrete layer, respectively. Details regarding the selection of the accelerometers and the strain gauges, the design of their positions, and the used installation procedures are described in Sections 3 and 4, respectively.

The thicknesses and mass densities of the layers were determined as follows. A precision laser was used to measure the actual layer thicknesses, see Table 1. They slightly deviate from the nominal values of Figure 2 because of execution tolerances. The mass densities of the two granular layers L2 and L3 were quantified in situ using the water replacement method. After digging a hole into the layer of interest, the excavated mass (measured by means of a portable digital scale) was divided by the volume of the hole. The volume was determined by laying a thin sheet of plastic into the hole, pouring water into it until the hole was

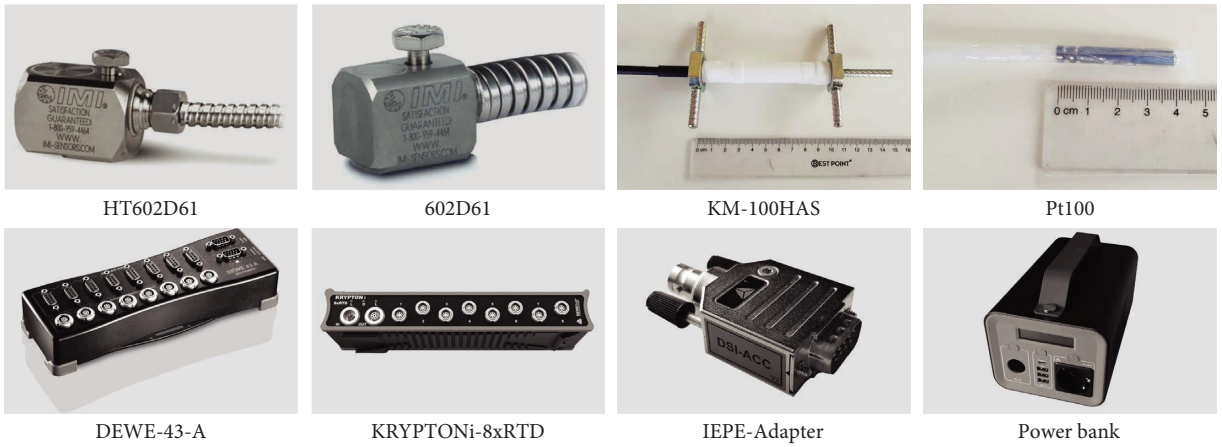

Figure 1: Accelerometers (HT602D61 and 602D61), strain gauges (KM-100HAS), temperature sensors (Pt100), and data acquisition system.

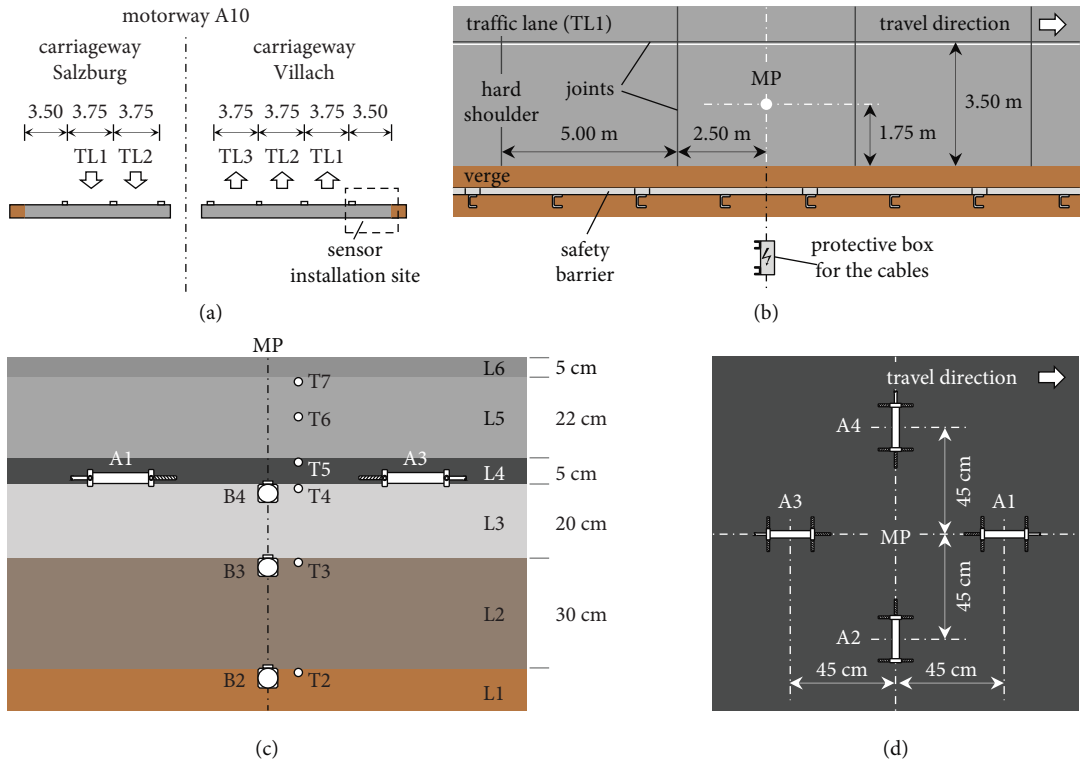

Note: The size of the sensors is exaggerated. MP, B, T and A stand for measuring point, accelerometer, temperature sensor and asphalt strain gauge.

Figure 2: Field-testing site #1 on motorway A10: (a) cross section through the motorway, (b) plan view onto the instrumented slab which was part of the emergency lane and MP = measurement point for FWD testing, (c) cross section of the pavement structure, nominal thicknesses of the layers, and depths of the installed sensors, and (d) plan view showing the in-plane positions and orientations of the strain gauges around the MP.

filled, and then measuring the volume of the water with a graduated cylinder. For both layers L2 and L3, the water replacement method was performed three times each, resulting in the mean values of the mass densities listed in Table 1. As for the layers L4, L5, and L6, samples of the three materials were collected during construction, see Table 1 for the mean values of the mass densities determined in the laboratory.

2.2. Field-Testing Site #2 on Motorway A3. Field-testing site #2 is a flexible pavement on the motorway A3, south of Vienna. Two nominally identical FWD measuring points were instrumented at a distance of approximately 70 m from each other, see Figure 3(b). Both measuring points are located in the middle of the hard shoulder which has the same design as the rest of the carriageway. The road section was rehabilitated as follows. The existing asphalt layers were removed. The existing

Table 1: Field-testing site #1: properties of the layers of the pavement structure, including nominal and actual measured thicknesses, h_{nom} and h_{meas}, respectively.

Layer	Name	Material	Binder ((mass)%)	h_{nom} (cm)	h_{meas} (cm)	Density (kg/m^3)
L6	Top-layer concrete	OB GK 8 (CEM II/B-S 42.5 N)	19.2	5.0	5.0	2305
L5	Bottom-layer concrete	UB GK 32 (CEM II/B-S 42.5 N)	15.6	22.0	22.0	2390
L4	Asphalt base course	AC 16 trag 70/100	4.7	5.0	8.2	2514
L3	Cement-stabilized granular layer	Cement and angular aggregates	—	20.0	17.6	2568
L2	Lower unbound granular layer	Angular aggregates	—	30.0	31.4	2595
L1	Subgrade	—	—	—	—	—

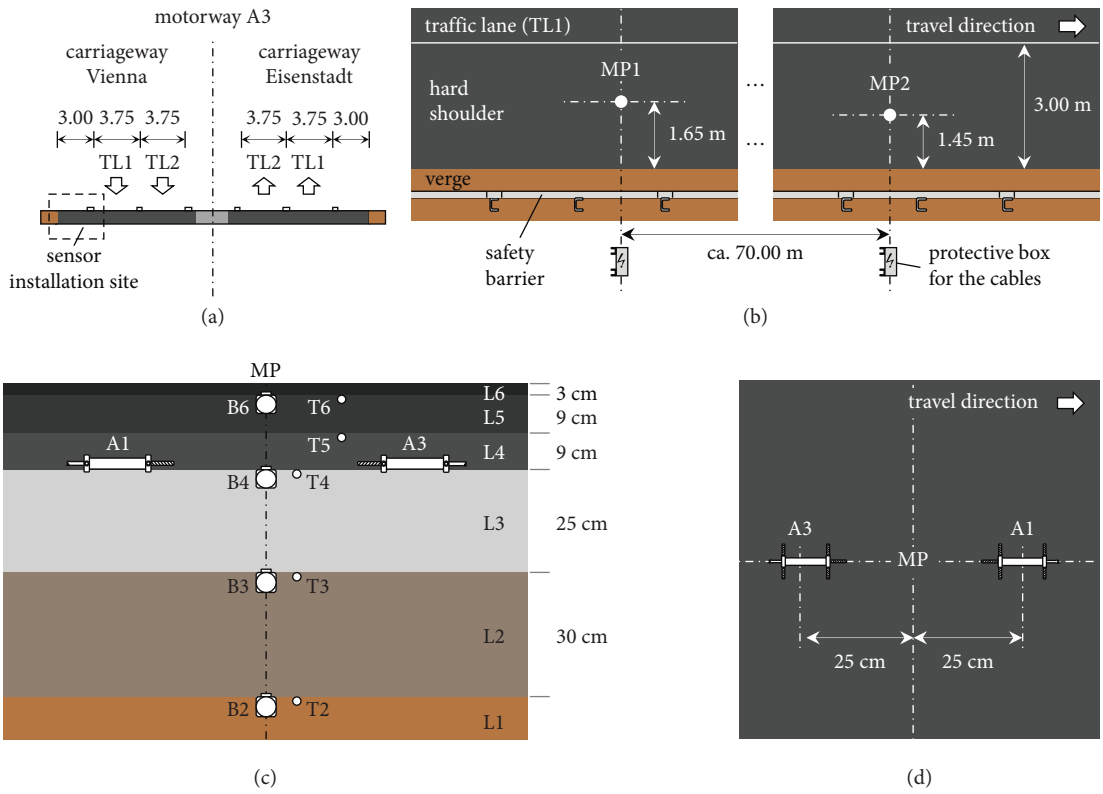

Note: The size of the sensors is exaggerated. MP, B, T and A stand for measuring point, accelerometer, temperature sensor and asphalt strain gauge.

Figure 3: Field-testing site #2 on motorway A3: (a) cross section through the motorway, (b) plan view onto the instrumented site which was part of the emergency lane and MP1 and MP2 denote measurement points for FWD testing, (c) cross section of the pavement structure, nominal thicknesses of the layers, and depths of the installed sensors, and (d) plan view showing the in-plane positions and orientations of the strain gauges around the MPs.

cement-stabilized layer (L3) was relaxed using a guillotine-type breaker followed by recompaction with a roller. This two-step "crack and seat" treatment reduced the potential for reflective cracking of three newly constructed asphalt layers. They are referred to as "base course L4," "binder course L5," and "surface course L6."

Sensors were embedded at several depths. Five temperature sensors (T2–T6) were placed at all interfaces between neighboring layers, see Figure 3(c). Four accelerometers (B2–B4 and B6) were installed along a vertical axis running through the measurement points (MP) for FWD testing, at the interfaces between the subgrade (L1), the unbound layer (L2), the cement-stabilized layer (L3), and the base course (L4), as well as between the binder course (L5) and the surface course (L6), see Figures 3(b) and 3(c). Two asphalt strain gauges (A1 and A3) were installed at the bottom of the base course, see Figure 3(d) for their symmetric arrangement relative to the measurement points. Two rather than four strain gauges were installed in order to reduce the number of embedded inhomogeneities, accounting for the fact that the asphalt layers have a significant load-carrying function in the pavement structure.

For the installation of sensors B2, T2, B3, and T3, rectangular areas with dimensions of $2.50 \times 2.50 \times 0.25$ m were excavated from the cement-stabilized layer L3, symmetrically with respect to the FWD measuring points, down to the surface of the unbound layer L2, see Figure 4. A smaller trench was excavated from the unbound layer L2 down to the surface of the subgrade L1, so that B2 and T2 could be installed. The material excavated from L2 was then reinserted and compacted with a vibrating plate compactor. The sensors B3 and

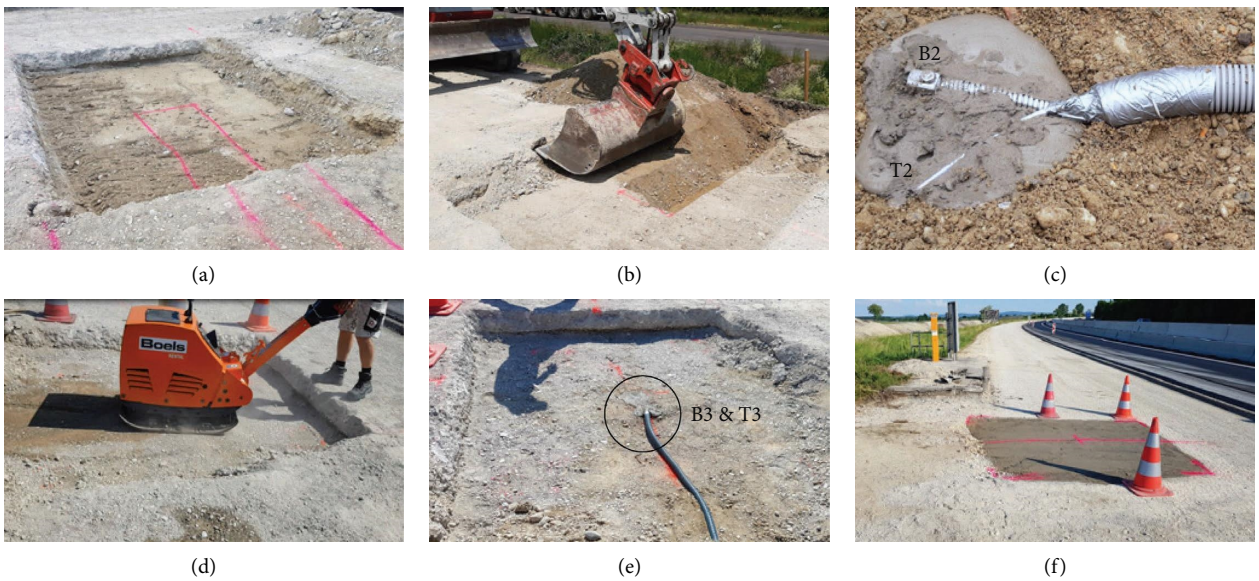

Figure 4: Installation of accelerometers in unbound granular layers on the motorway A3: (a) excavation of the cement-stabilized layer, (b) smaller excavation of the unbound layer down to its boundary with the subgrade, (c) installation of sensors at the surface of the subgrade, (d) refilling and compaction of granular material, (e) installation of sensors at the surface of the unbound layer, and (f) placement of lean concrete.

T3 were installed. The volume excavated from L3 was filled with lean concrete rather than with the excavated material because it was impossible to reinsert the excavated material in a way that would have led to properties similar to those of the relaxed cement-stabilized layer. Sensors B4 and T4, as well as the strain gauges, were installed shortly before the placement of the base course L4. The temperature sensor T5 was installed immediately after the construction of the base course L4. The sensors T6 and B6 followed immediately after the construction of the binder course L5. Details regarding the selection of the accelerometers and the strain gauges, the design of their positions, and the used installation procedures are described in Sections 3 and 4, respectively.

The thicknesses of the layers and the mass-density of the unbound layer L2, see Table 2, were determined using the same methods as described for field-testing site #1. In situ cast cubes of lean concrete (L3) and fresh-mix samples of all three asphalt layers (L4–L6) were collected for laboratory testing. The mass densities of these materials are listed in Table 2.

2.3. Field-Testing Site #3 on Expressway S31. Field-testing site #3 is a flexible pavement on the expressway S31 in the federal state Burgenland. In the absence of a hard shoulder, the FWD measuring point was installed in the middle of the right lane (TL1), see Figure 5. There, predominantly heavy-vehicle traffic is expected. In the longitudinal direction, the instrumented site is located after a breakdown bay. This position (i) facilitated the installation of sensors and (ii) renders in situ testing convenient and safe for the experimenters. The rehabilitation treatment comprised (i) the renewal of the asphalt pavement and (ii) widening of the carriageways including the introduction of a central reserve. The instrumented pavement structure consists of three asphalt layers resting on two unbound layers which are so similar that the interface between them could not be identified.

Sensors were embedded at several depths. Three temperature sensors (T2, T4, and T6) were placed at the interfaces between (i) the subgrade (L1) and the lower unbound layer (L2), (ii) the upper unbound layer (L3) and the base course (L4), as well as (iii) the binder course (L5) and the surface course (L6), see Figures 5(b) and 5(c). Temperature sensor T5 was installed at the interface between the base and binder courses. Three accelerometers (B2, B4, and B6) were installed along a vertical axis running through the central measurement point (MP) for FWD testing, at the same interfaces as T2, T4, and T6. Two asphalt strain gauges (A1 and A3) were installed into the base course, see Figure 5(d) for their symmetric arrangement relative to the measurement point. Again, two rather than four strain gauges were installed in order to keep the number of embedded inhomogeneities at a reasonable minimum.

The sequence of installation of the sensors B2–B4, T2, and T4–T6 was the same as in the other field-testing sites. The asphalt strain gauges, however, were installed at the *top* of the base course. This was part of an installation strategy which was specifically aimed at ensuring the position accuracy of the strain gauges. Details regarding the selection of the accelerometers and the strain gauges, the design of their positions, and the used installation procedures are described in Sections 3 and 4, respectively.

The thicknesses of the layers and the mass density of the unbound layers L2 and L3 were determined using the same methods as described for field-testing site #1. Samples from all three asphalt layers (L4–L6, fresh mix) were collected for laboratory testing. The mass densities of these materials are listed in Table 3.

Table 2: Field-testing site #2: properties of the layers of the pavement structure, including nominal and actual measured thicknesses for both measuring points, h_{nom}, h_{meas}^{MP1}, and h_{meas}^{MP2}, respectively.

Layer	Name	Material	Binder (mass %)	h_{nom} (cm)	h_{meas}^{MP1} (cm)	h_{meas}^{MP2} (cm)	Density (kg/m^3)
L6	Asphalt surface course	SMA 11 deck PmB 45/80-75	5.8	3.0	3.7	3.7	2515
L5	Asphalt binder course	AC 22 bin PmB 25/55-65	4.3	9.0	8.6	8.7	2420
L4	Asphalt base course	AC 22 bin PmB 45/80-65	4.2	9.0	8.8	8.3	2500
L3	Cement-stabilized granular layer (lean concrete)	C8/10 GK16 (CEM II/A-M 42.5N)	—	25.0	23.0	33.0	2165
L2	Unbound granular layer	Angular aggregates	—	30.0	30.0	33.0	2455
L1	Subgrade	—	—	—	—	—	—

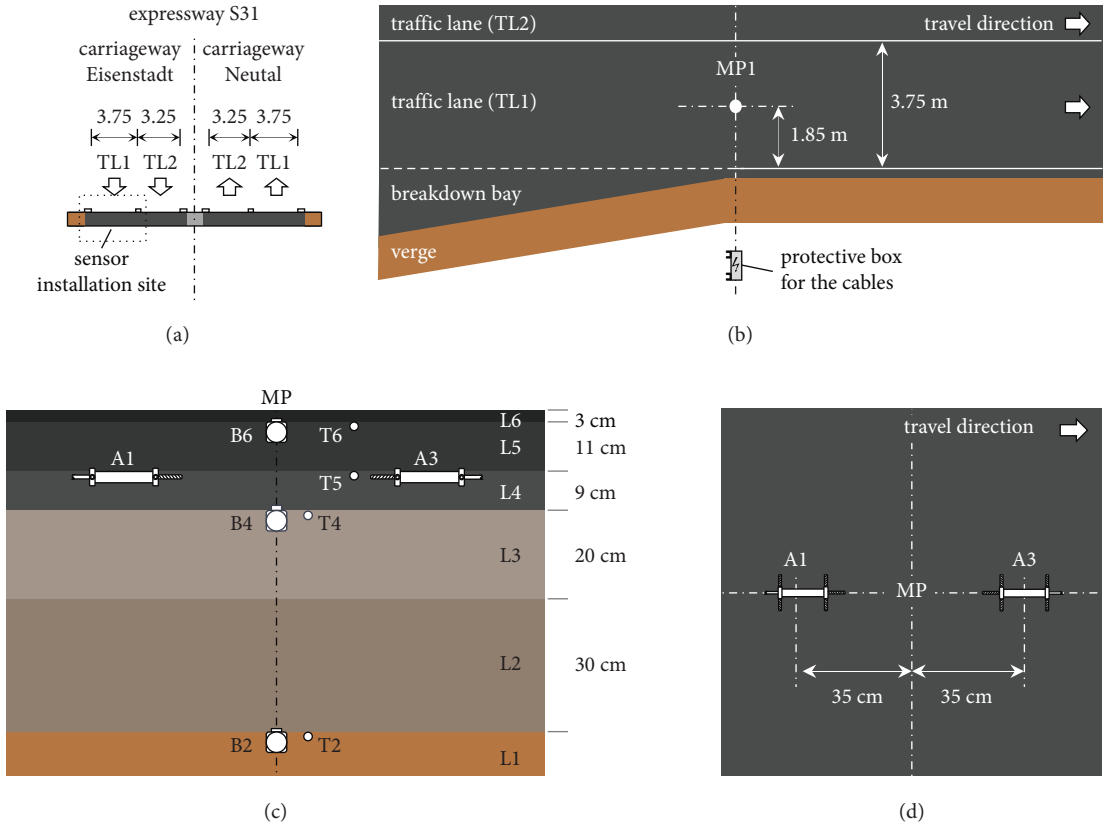

Note: The size of the sensors is exaggerated. MP, B, T and A stand for measuring point, accelerometer, temperature sensor and asphalt strain gauge.

Figure 5: Field-testing site #3 on expressway S31: (a) cross section through the motorway, (b) plan view onto the instrumented site which was part of the right traffic lane and MP = measurement point for FWD testing, (c) cross section of the pavement structure, nominal thicknesses of the layers, and depths of the installed sensors, and (d) plan view showing the in plane positions and orientations of the strain gauges around the MP.

Table 3: Field-testing site #3: properties of the layers of the pavement structure, including nominal and actual measured thicknesses, h_{nom} and h_{meas}, respectively.

Layer	Name	Material	Binder (mass %)	h_{nom} (cm)	h_{meas} (cm)	Density (kg/m^3)
L6	Asphalt surface course	SMA 11 deck PmB 45/80-65	5.8	3.0	4.0	2515
L5	Asphalt binder course	AC 32 bin PmB 45/80-65	4.0	11.0	11.9	2413
L4	Asphalt base course	AC 22 bin PmB 45/80-65	4.3	9.0	11.0	2416
L3	Upper unbound granular layer	Angular aggregates (basalt)	—	20.0	*	2590
L2	Lower unbound granular layer	Rounded aggregates	—	30.0	*	2720
L1	Subgrade	—	—	—	—	—

*No clear division was found between layers L2 and L3. Only a total thickness of h_{meas} = 55.4 cm was reported.

3. Installation of the Accelerometers

3.1. State-of-the-Art Applications. Two types of accelerometers have been mainly used in past pavement applications: integrated electronics piezoelectric (IEPE) and micro-electromechanical system (MEMS) accelerometers. IEPE sensors are mainly used to capture dynamic events, exhibiting a frequency range of some 0.3 Hz–10 kHz. They consist of a fixed mass, a piezoelectric material (e.g., quartz or a piezoceramic), and an integrated signal amplifier to reduce noise [57, 58]. If acceleration is imposed on the sensor, the mass will be pressed against the piezoelectric element. The generated electric charge can be measured and correlated to the acceleration. MEMS sensors, in turn, are used for dynamic and low-frequency measurements and are also applicable for frequencies smaller than 0.3 Hz. MEMS accelerometers are either based on measurements of changes in electrical capacitance (capacitive sensors), or they use strain gauges (piezoresistive sensors), see [57, 59].

Accelerometers were mounted in several studies to the surface of pavement structures in order to measure acceleration histories either caused by real traffic or by load simulators. The measured acceleration histories were used as reference values for the optimization of dynamic simulations of the behavior of pavement structures [38, 60]. Measured acceleration histories were also converted, by means of double time-integration, into

deflection histories, see [14, 55, 61–64]. The deflections were then used for back-calculation of layer properties. Accelerometers positioned on the pavement surface have also been used in the context of surface wave testing, see [65–70]. Depending on the used technique, surface wave pavement testing allows either for direct determination of the modulus of the top paving layer or for the estimation of the modulus of each layer through a back-calculation analysis.

In this study, accelerometers are used to determine the time of flight of longitudinal waves propagating vertically through these layers. This way, the theory of elastic wave propagation through isotropic elastic media can be used for the direct quantification of layer moduli [71, 72, 73].

3.2. Theoretical Fundamentals. Three types of stress waves are generated when hitting a pavement structure vertically at its surface. Longitudinal waves mainly propagate vertically downwards. They are also referred to as compression or *P*-waves. Particle displacements are aligned with the direction of wave propagation. Transversal waves mainly propagate diagonally downwards. They are also referred to as shear or *S*-waves. Particle displacements are normal to the direction of wave propagation. Longitudinal and transversal waves are partly reflected and refracted at the interfaces between different layers [74]. Rayleigh waves travel along the surface. They are also referred to as surface or *R*-waves. Herein, the focus rests on longitudinal waves.

Depending on the amplitude of stress waves, they may be either *elastic*, provided that they induce *reversible* deformation only, or inelastic, provided that also irreversible deformations take place. The wave propagation front, in turn, always refers to an elastic wave because it is faster than inelastic waves [75]. The present study takes advantage of this property.

Herein, accelerometers are installed both at the top and at the bottom of layers of interest in order to determine the time of flight, Δt, of the front of a longitudinal wave which propagates vertically through these layers. Based on measured values of Δt, the velocity of the longitudinal wave, v_L, can be quantified as

$$v_L = \frac{h}{\Delta t}, \tag{1}$$

where h denotes the thickness of the layer of interest.

Quantification of the elastic stiffness of the layer based on its longitudinal wave velocity is facilitated by two realistic assumptions: (i) the layer is idealized as a macrohomogeneous material and (ii) the longitudinal wave is considered to be a bulk (rather than a bar) wave, meaning that the lateral deformation is prevented (rather than free). Under these premises, the theory of elastic waves propagating through isotropic media delivers the following relation between the component C_{1111} of the elastic stiffness tensor, the mass density ρ of the material, and v_L of equation (1):

$$C_{1111} = \rho v_L^2. \tag{2}$$

Assuming the layer material to be isotropic and its Poisson's ratio ν to be known, the following standard relation of isotropic elasticity allows for quantification of the modulus of elasticity E:

$$E = C_{1111}\frac{(1+\upsilon)(1-2\upsilon)}{(1-\upsilon)}. \tag{3}$$

3.3. Sensor Selection. IEPE accelerometers 602D61 and HT602D61 by PCB with stainless steel housing and a ceramic sensing element, see Figure 1, comply with the requirements of the present study. They are suitable in terms of measurement range and resolution, they are reasonably small, and they have a sufficient resistance against (i) mechanical impact during compaction and (ii) high temperatures during construction of asphalt layers. The side exit of the sensors together with a 3 m armored jacketed sleeve provide the high level of protection for the connector and the cable, which is required in the present application. In more detail, the sensors 602D61 have dimensions of 25.4 mm × 18.8 mm × 25.4 mm ($L \times W \times H$), a temperature range of −54 to +121°C, and a frequency range of 0.5 Hz to 8000 Hz. The high-temperature sensors HT602D61 have dimensions of 26.9 mm × 25.4 mm × 30.2 mm, a temperature range of −54 to +162°C, and a frequency range of 0.8 Hz to 8000 Hz. The sensitivity and the amplitude range of both sensors amount to 10.2 mV/(m/s^2) and to ±490 m/s^2, respectively.

3.4. Data Acquisition Rate and System. A suitable data acquisition rate had to be selected in order to ensure that the time of flight of a longitudinal wave propagating through a layer of interest can be determined with acceptable accuracy. In order to achieve a measurement accuracy of at least 10%, it is necessary to record at least 10 acceleration values while a longitudinal wave travels from the accelerometer at the top of a layer to the accelerometer at the bottom of the same layer. This calls for the data acquisition rate which is by factor of at least 10 larger than the inverse of the estimated time of flight of the elastic wave through the layer of interest. In order to estimate times of flight a priori, equations (1)–(3) were evaluated for the designed thicknesses of the layers, see Tables 1–3, and values of the elastic modulus, Poisson's ratio, and mass density of each layer of interest were taken from the literature [76–80], see Table 4. For asphalt and unbound materials, upper and lower bounds of the elastic modulus, representative for winter and summer conditions, respectively, were taken into account. The stiffness properties of the concrete and cement-stabilized layers were assumed to remain virtually constant within the temperature range investigated [81]. The estimated times of flight are listed in Table 4.

(1) At the field-testing site #1 on the A10, three accelerometers were installed: at the bottom of the unbound layer L2, at the interface between L2 and the cement-stabilized layer L3, and at the top of L3, see Figure 2. This allows for in situ stiffness characterization of layers L2 and L3. The required data acquisition rate required is equal to 74 kHz, see Table 4 (as for quantification of the stiffness properties of the

concrete and asphalt layers, samples were taken for laboratory testing).

(2) At the field-testing site #2 on the A3, four accelerometers were installed: at the bottom of the unbound layer L2, at the interface between L2 and the lean concrete layer L3, at the interface between L3 and the asphalt base course L4, and at the top of the asphalt binder course L5, see Figure 3. This allows for in situ stiffness characterization of layers L2 and L3 as well as of the sandwich layer consisting of the asphalt base and binder courses (L4 and L5). The required data acquisition rate required is related to the high stiffness of asphalt exposed to winter temperatures. It is equal to 169 kHz, see Table 4.

(3) At the field-testing site #3 on the S31, three accelerometers were installed: at the bottom of the lower unbound layer L2, at the interface between the upper unbound layer L3 and the asphalt base course L4, and at the top of the asphalt binder course L5, see Figure 5. This allows for in situ stiffness characterization of two sandwich layers. They consist of the unbound materials (L2 and L3) and of the asphalt base and binder courses (L4 and L5), respectively. The required data acquisition rate is equal to 154 kHz, see Table 4.

The USB data acquisition system DEWE-43-A, see Figure 1, with a data acquisition rate of 200 kHz and eight fully synchronized channels complies with the requirements of all three field-testing sites. DEWE-43-A supports voltage and full-bridge signals without additional adapters, as well as IEPE, charge, thermocouples, half-bridge, quarter bridge, RTD, current, resistance, and LVDT signals with the help of DSI adapters. Thus, the DEWE-43-A is capable of simultaneously acquiring data from four strain gauges and four accelerometers. DSI-ACC adapters were required for powering the IEPE accelerometers with the required directed current. As for the ACC, a BNC adapter RS 124–2521 was used.

3.5. Sensor Installation. Installing accelerometers at *multiple depths during the construction* of the pavement represented a novel challenge, differing from the installation at a *single* depth and *after* construction as described in [14, 38, 62, 64]. As for the present study, the following two requirements had to be fulfilled:

(1) The sensors must remain in place and deliver a reliable signal after the installation and compaction of subsequent layers of the pavement structures

(2) The sensors must be aligned along a vertical axis, such that the longitudinal wave, produced by hitting the surface of the completed pavement right above the sensors, propagates downwards along this axis

The installation of the accelerometers in unbound granular layers (B2 and B3) was conducted as follows, see also Figure 4. The starting level was that of the unbound layers, given that they remained in place during the rehabilitation works on all three field-testing sites. For the installation of the lowest sensors B2 and T2, an excavator was used to reach the boundary between the unbound layer L2 and the subgrade L1. Layer-wise excavation allowed for separating different materials in order to refill the trenches later with the right excavation materials. In a first step, the excavation reached the boundary between L2 and L3, see Figure 4(a). In a second step, a smaller trench was created reaching the boundary between L2 and L1, see Figure 4(b). At this level, sensors B2 and T2 were embedded using a quick-setting cement mortar that served two goals: (i) to prevent a displacement of the sensor or a disconnection of the cable and (ii) to protect the sensor from direct contact with (tips of) large aggregates, since concentrated loads could damage the sensors, see Figure 4(c). The exact horizontal and vertical position of all sensors was determined using a measuring tape and a precision laser, respectively. Two independent permanent reference points were used. The cables from both sensors were placed in a protection tube starting approximately 30 cm away from the sensors. In the next step, the excavation material from layer L2 was reinserted in the smaller trench, and the layer was compacted using a vibrating plate, see Figure 4(d). At the interface between L2 and L3, sensors B3 and T3 were installed similarly, see Figure 4(e). Finally, the remaining trench was closed with the excavation material from L3 and compacted. Only in the case of the second field-testing site on the A3 motorway, as described in Section 2, a new material was inserted, see Figure 4(f).

High-temperature accelerometers were installed at the interfaces between asphalt layers and the cement-stabilized or lean concrete layers (B4 and B6). The procedure is illustrated in Figure 6 and described next. First, openings for the sensors and grooves for the cables were cut in the cement-stabilized or lean concrete layers, see Figure 6(a). Then, the sensors were fixed and the cables were covered using quick-setting mortar, see Figure 6(b). Right before paving, the sensors were first covered with loose asphalt mixture, followed by careful compaction with a hand tamper, see Figure 6(c). This provided protection to the sensor against high compaction forces and slightly reduced the temperature of the material in contact with the sensor. Special care was taken so that delivery trucks and, especially, the track chain of the paver did not drive over the positions of the sensors. The plastic tubes protecting the cables were used only outside of the bound layers (starting from the edge of the pavement) in order to minimize potential weak spots and cavities.

For the installation of the accelerometers between two asphalt layers (B6), the opening for the sensor and the groove for the cable were produced *during* the construction of the lower asphalt layer. This was achieved by pushing a steel dummy of the sensor and a steel pipe as placeholders for the sensor and the cable into the surface of the freshly placed asphalt, followed by regular compaction with rollers. Later, the dummy and the pipe were removed, and the sensor together with its cable could be simply inserted into the opening and the groove, see Figures 6(d) and 6(e). Before

Table 4: Design calculations: data acquisition rates required for reliable measurements of the times of flight of elastic waves passing vertically through individual layers of all three field-testing sites.

Layer	Thickness (cm)	E-modulus (MPa)	Poisson's ratio (-)	Density (kg/m^3)	Velocity (m/s)	Time of flight Δt (s)	$1/\Delta t$ (s^{-1})	Req. rate of data acquisition (kHz)
Field-testing site #1 on motorway A10								
L6	5	30,000	0.20	2,305	3,803	1.31×10^{-5}	76,056	761
L5	22	30,000	0.20	2,390	3,735	5.89×10^{-5}	16,975	170
L4 (W)	5	16,000	0.30	2,514	2,927	1.71×10^{-5}	58,540	585
L4 (S)	5	1,300	0.30	2,514	834	5.99×10^{-5}	16,687	167
L3	20	5,000	0.20	2,568	1,471	1.36×10^{-4}	7,354	74
L2 (W)	30	800	0.35	2,595	703	4.27×10^{-4}	2,345	23
L2 (S)	30	200	0.35	2,595	352	8.53×10^{-4}	1,172	12
Field-testing site #2 on motorway A3								
L6 (W)	3	18,000	0.30	2,515	3,104	9.70×10^{-6}	103,465	1,035
L6 (S)	3	2,400	0.30	2,515	1,133	2.65×10^{-5}	37,780	378
L5+L4 (W)	18	17,000	0.30	2,459	3,051	5.90×10^{-5}	16,948	169
L5+L4 (S)	18	1,850	0.30	2,459	1,006	1.79×10^{-4}	5,591	56
L3	25	5,000	0.20	2,165	1,602	1.56×10^{-4}	6,408	64
Field-testing site #3 on expressway S31								
L5+L4 (W)	20	17,000	0.30	2,414	3,079	6.50×10^{-5}	15,395	154
L5+L4 (S)	20	1,850	0.30	2,414	1,016	1.97×10^{-4}	5,078	51
L3+L2 (W)	50	915	0.35	2,655	744	6.72×10^{-4}	1,487	15
L3+L2 (S)	50	220	0.35	2,655	365	1.37×10^{-3}	729	7

Note: L2 of A3 is equal to L2 of A10; L6 of S31 is equal to L6 of A3; (W) = winter; (S) = summer; the times of flight for the layers printed in bold face can be measured reliably with a data acquisition rate of 200 kHz.

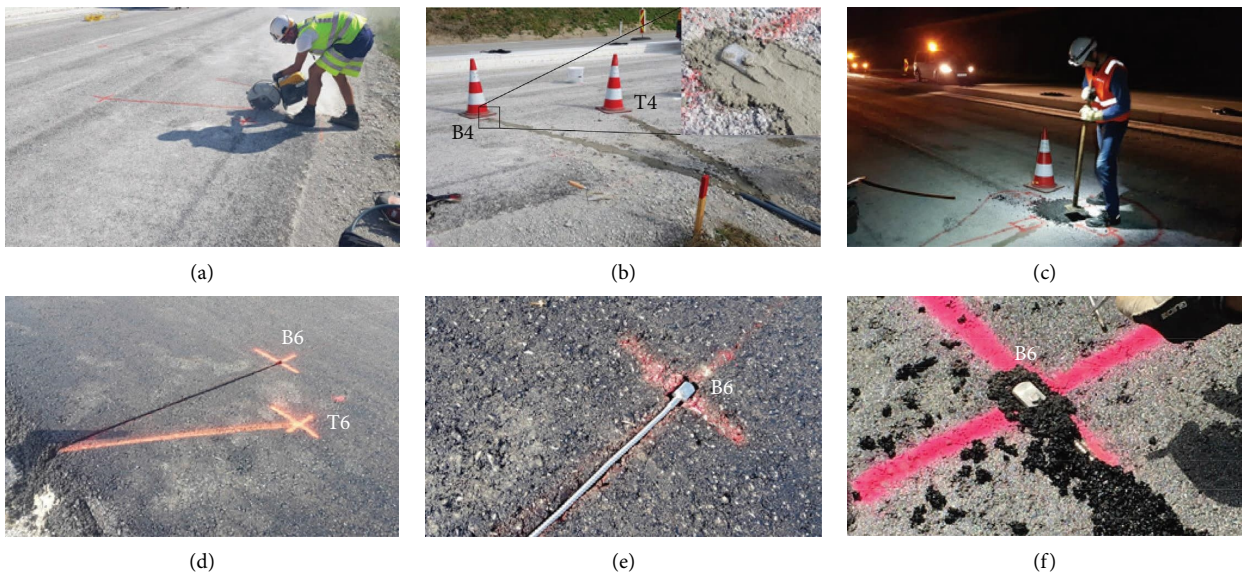

(a) (b) (c)

(d) (e) (f)

Figure 6: Installation of accelerometers on top of the cement-stabilized layer of motorway A10, see (a)–(c), and on top of an asphalt layer of motorway A3, see (d)–(f), respectively: (a) groove cutting for sensors and cables, (b) installation with quick-setting cement mortar, (c) hand compaction of small asphalt sample as protection prior to paving, (d) groove for sensor and cable, (e) placement of accelerometer in the groove, and (f) compaction with fine-grained asphalt material.

the construction of the next layer, a small quantity of loose asphalt was sieved using a standard sieve to obtain a material with a grain size smaller than 8 mm. The sieved material was used to fill remaining cavities and to cover the accelerometer with approximately 1 cm of asphalt as a protective measure, see Figure 6(f). Then, the unsieved material was piled on the sensors and compacted manually, as shown in Figure 6(c). The new asphalt layer was afterwards paved as usual.

All but two of the installed accelerometers deliver reliable signals under dynamic loads. The exact reason why sensors B2 on the A10 and B6 of the S31 do not work remains unknown. It is speculated that either the sensor, and/or the sensor-cable connection, and/or the cable was/were mechanically damaged during construction.

4. Installation of the Asphalt Strain Gauges

4.1. State of the Art Applications. Asphalt strain gauges have been successfully employed in the context of pavement testing [82–84], monitoring of instrumented sections [85, 86], studies of stiffness properties of layers [87, 88], and in comparing vehicle loads with FWD tests [89]. The performance of KM-100HAS and other asphalt strain gauges has been compared in full-scale experiments under controlled loading and temperature conditions [90]. Different installation methods have been studied in a project involving 374 strain gauges which were used to monitor pavements over a period of four years [91].

In this study, the measurements of the asphalt strain gauges are used for validation of numerical simulations of the pavement structure subjected to FWD loading. In addition, they allow for detecting anomalous FWD results, such as obtained when the slab is curling.

4.2. Sensor Selection. KM-100HAS asphalt strain gauges by Tokyo Measuring Instruments were installed, see Figure 1. They have a temperature range from −20°C to +180°C, an amplitude range of ±5000 μm/m, and a measurement length of 100 mm. These sensors have reinforcing bars at both ends, see Figure 1. They ensure a firm embedment in asphalt. The used data acquisition system, DEWE-43-A, provides a 5 V (350 Ω) excitation for full bridge sensors. This is larger than the recommended voltage (2 V) but smaller than the allowable bridge excitation for KM-100HAS (10 V).

4.3. Design of the Installation Position of the Strain Gauges. The installation positions of the strain gauges were decided based on the results of linear elastic, static, and axisymmetric finite element (FE) simulations of an FWD experiment on multilayered pavement structures performed with ABAQUS [92]. For each one of the three field-testing sites, a customized simulation was performed. The elastic properties of the layers were taken from Table 4. The imposed FWD forces were set equal to 200 kN for field-testing site #1 and to 150 kN otherwise. These forces were selected based on experience and according to the Austrian FWD standard stating that in the case of very stiff pavement structures, the applied force should be increased until that the magnitude of the measured deflections exceeds 0.020 mm (at $r = 1.80$ m) [93]. It was also considered that this requirement should be satisfied even in the winter months. Exemplary FE results for the field-testing site #3 (winter simulation) are shown in Figure 7, whereby the used pavement and load model is depicted in Figure 7(a).

The essential results from the FE simulations are the radial normal strains of asphalt, as a function of the distance from the center of the falling weight, in the specific depths from the

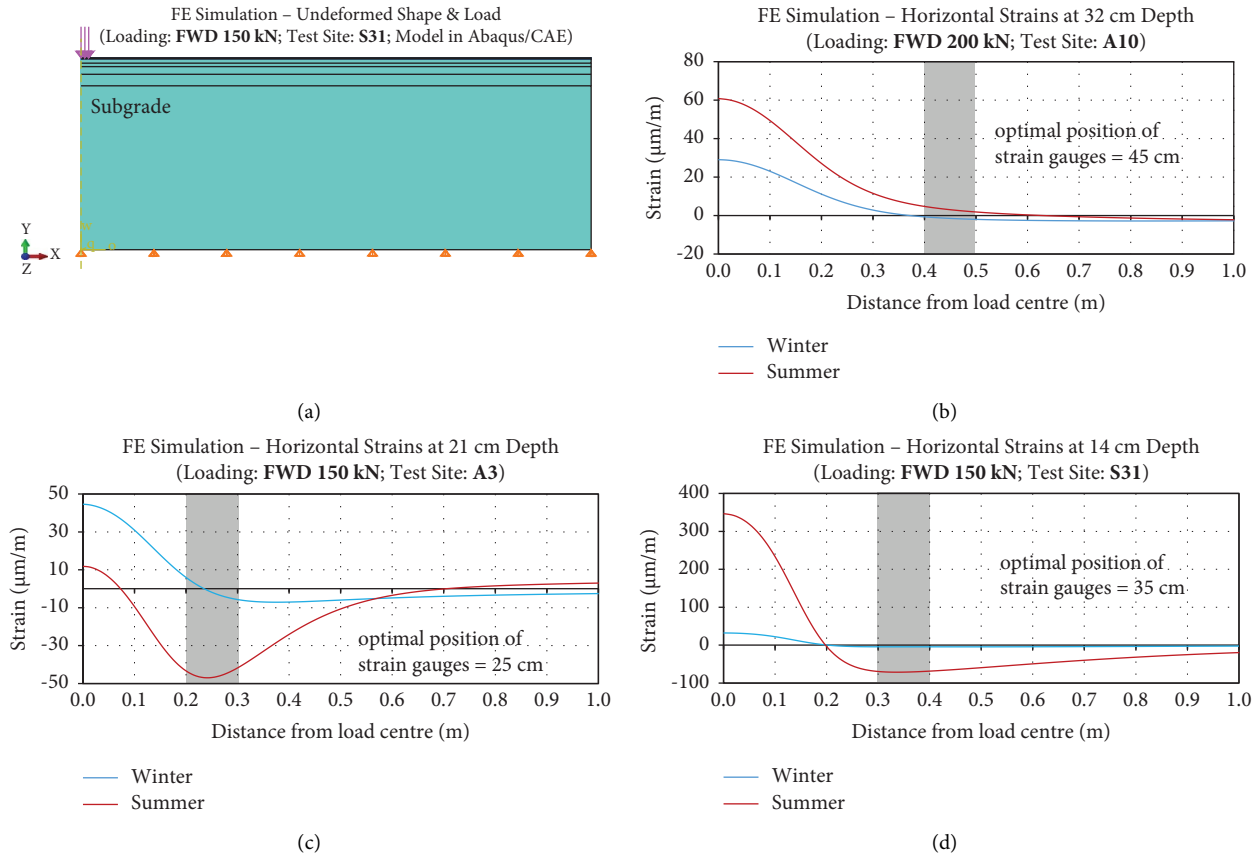

Figure 7: Results of radial-symmetric FE simulations providing input for the decision-making process regarding the installation positions of the asphalt strain gauges: (a) pavement and load model of testing site #3 on the S31, as well as radial normal strains as a function of the distance from the center of the falling weight in specific depths of the pavement structures of field-testing sites (b) #1 on the A10, (c) #2 on the A3, and (d) #3 on the S31.

surface of the pavement structures, in which the sensors were installed, see Figures 7(b)–7(d). The horizontal distance of the asphalt strain gauges from the center of the falling weight was determined based on the following four considerations: (i) the strain shall be sufficiently large to obtain reliable measurements; (ii) the strain gradients at the position of the sensors should be reasonably small, such that the measurements are easy to interpret; (iii) the difference between the simulated strain during summer and winter should be sufficiently large, such that the measurements will capture seasonal variations; and (iv) the sensors should not be installed too near to the load center to limit a potential influence on the flight-time measurement. Based on trade-offs between these considerations, it was decided to install the strain gauges in horizontal distance from the center of the falling weight amounting to 45 cm for testing site #1 on the A10, to 25 cm for testing site #2 on the A3, and to 35 cm for testing site #3 on the S31.

4.4. Installation Method A: Cut, Install, and Cover after Asphalt Placement. Installation method A was applied at the field-testing site #1 on the A10, see the schematic overview in Figure 8(a). The installation method is similar to the trench-cut method described in [91], with the difference that we used *the same* asphalt mixture to fill the holes which were excavated in order to place the sensors (rather than a different material as in [91]). The installation began immediately after the placement of the asphalt mixture and the first roller pass, see Figures 8(a)-A and 9(a). The position of the four strain gauges was marked, see Figure 9(b). The openings for the sensors and grooves for the cables were excavated using a pickaxe, a geological hammer and a shovel, see Figure 9(c). These openings reached down to the cement-stabilized layer on top of which the asphalt layer was constructed, see Figure 8(a)-B. The manufacturer of the strain gauges recommends covering the sensors with asphalt having a maximum aggregate size of 5 mm. Therefore, a standard sieve was used to decrease the maximum aggregate size of hot asphalt, directly taken from the auger of the paver, from 16 mm to smaller than 8 mm, see Figure 9(d). Sieving worked best when using a short wooden plank to press the material through the sieve. From the sieved material, 1 cm thick asphalt beds were produced, the strain gauges were placed on top, and their vertical position was measured, see Figures 8(a)-C and 9(e). The sensors were covered with another 1 cm thick layer of the sieved material. Finally, the opening was closed using the regular asphalt with a maximum aggregate size of 16 mm. Compaction was started by hand with a tamper and continued with a roller, see Figure 8(a)-D. In the immediate vicinity of the installed strain gauges, the roller was operated in the static mode rather than in the vibrating mode.

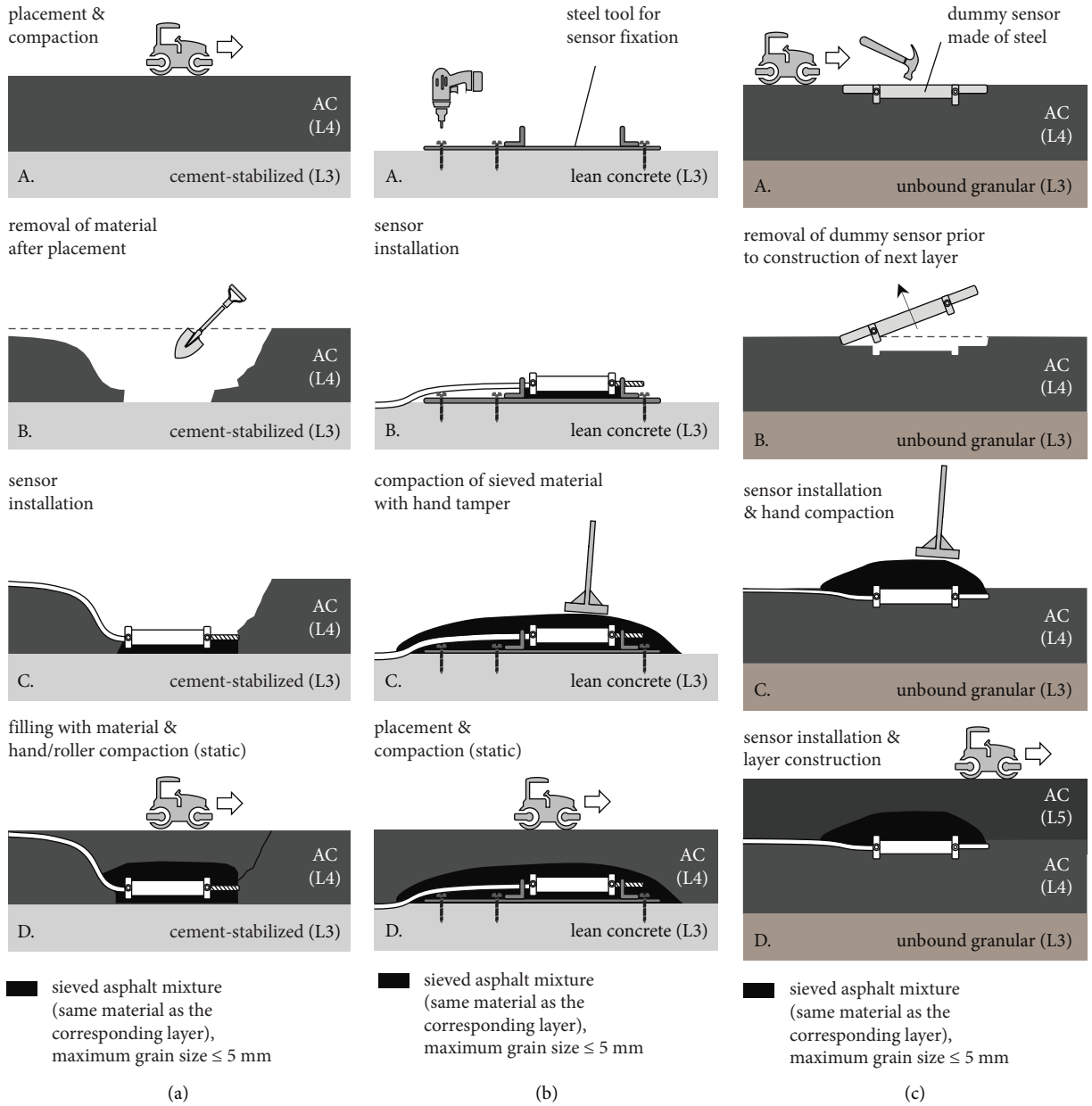

Figure 8: Overview of the three methods used for installation of asphalt strain gauges: (a) method A (A10), (b) method B (A3), and (c) method C (S31).

The following experience was gained with installation method A. Its main advantages are the position accuracy of the sensors and the low potential for damage during construction. The main disadvantages are problems related to rather fast cooling of the asphalt. It made the installation process quite stressful, and it got progressively more difficult to work with the material. These problems manifest themselves in visible imperfections regarding the uniformity of the asphalt layer in the region of the field-testing site, see Figure 9(f). While these imperfections are most probably the result of delayed compaction, they are rather unproblematic in the case of field-testing site #1, since a concrete slab was later placed on top of the asphalt layer. At the field-testing sites #2 and #3, however, the asphalt base course serves a much more important role in the behavior of the pavement structures. Therefore, installation method B was designed and used for field-testing site #2.

4.5. Installation Method B: Installation in a Fixation Tool, before Asphalt Placement. Installation method B was applied at both measuring points of the field-testing site #2 on the A3, see Figure 8(b). The installation method is an extension of the mound method described in [91]. A device was developed and produced to ensure the position stability of the strain gauges during construction, see Figure 10(a). The device consisted of two L-shaped metal bars that were fixed to a 30 cm flat stainless steel flat bar. Cuts in the vertical parts of

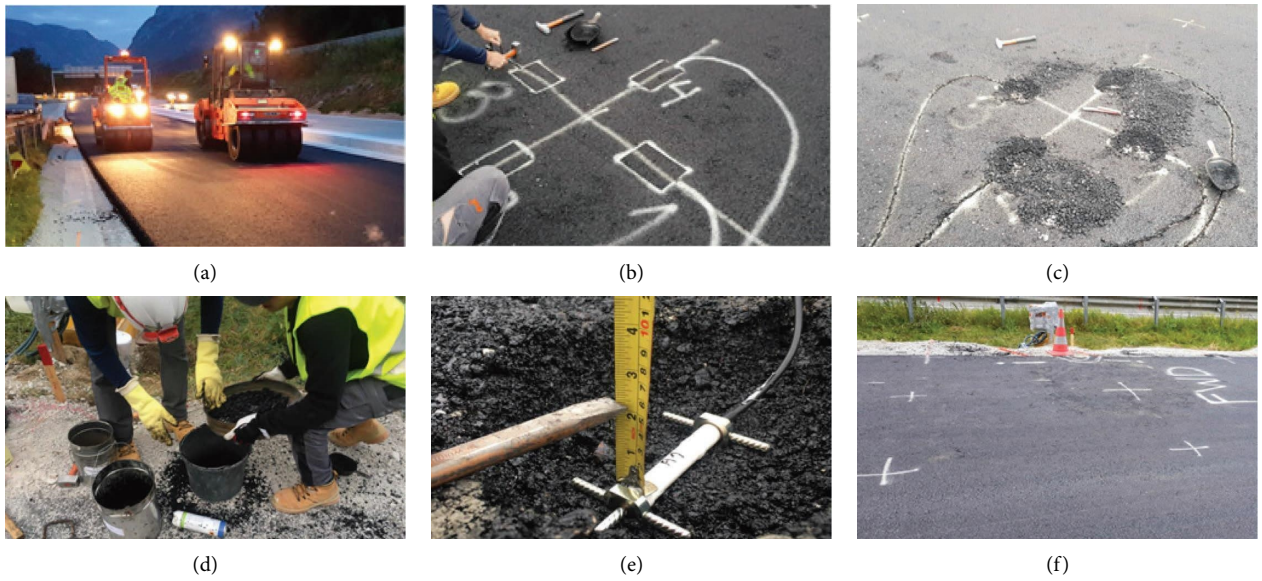

FIGURE 9: Installation of asphalt strain gauges at field-testing site #1 on the A10 using method A: cut, install, and cover after asphalt placement.

the L-shaped bars ensured that an asphalt strain gauge fitted into the fixation device. The distance between the two L-shaped bars was designed to be slightly longer than the length of the sensor, leaving room in longitudinal direction for the strain gauge to operate without constraints. The vertical parts of the L-shaped bars had openings for the cable and the axial reinforcing bar of the sensor, respectively. One day before the asphalt paving, the device was screwed onto the underlying lean concrete layer, see Figures 8(b)-A and 10(b). Wooden planks were installed temporarily to prevent construction vehicles from accidentally driving over the device. Right before asphalt placement, a 1 cm thick bed made of sieved asphalt (see also Subsection 4.4) was placed on the device, and the strain gauge was installed on top of it, see Figure 8(b)-B. The openings of the vertical parts of the L-shaped bars were closed with wire in order to prevent possible vertical movements of the sensors, see Figure 10(c). Thus, the fixation device prevented rigid body motions of the asphalt strain gauge, but in a way that allows the sensor to operate without constraints. The sensors were covered, first with sieved material, see Figures 8(b)-C and 10(d), and then with loose asphalt mixture around a larger area in order to protect the sensors from damage associated with laydown and compaction, see Figure 10(e). During the paving process, care was taken to ensure that the construction machines did not drive over the sensors, see Figure 10(f). Roller compaction in the area near the sensors was conducted in the static mode than in the vibrating mode, see Figure 8(b)-D.

The following experience was gained with installation of method B. Its main advantage is that the asphalt strain gauges remained in their desired positions during installation and compaction of the asphalt layer. The main disadvantage is that despite the numerous steps taken to protect the asphalt strain gauges, only two out of four sensors work now that the construction work is finished. Therefore, installation method C was designed and used for field-testing site #3, with the aim to protect strain gauges from damage during compaction.

4.6. Installation Method C: Use of Steel Dummy Place-Holders for the Real Sensors. Installation method C resembles the installation of accelerometers in asphalt layers, see Subsection 3.5 and Figure 8(c). Before installation, steel dummy sensors were produced, see Figure 11(a). They had the same dimensions as the actual strain gauges.

The installation method works only if the strain gauges are installed at the top of a freshly built asphalt layer, rather than at the bottom (as done at the field-testing sites #1 and #2). The installation process began right after the placement of the asphalt base layer, but before its compaction. The steel dummies were hammered into the asphalt at the positions where the strain gauges should be finally located, see Figures 8(c)-A and 11(b). Then, the rollers compacted the asphalt in the vibrating mode, without paying special attention to the steel dummies, see Figure 8(c)-A. One day before placement of the next asphalt layer (=asphalt binder course), the steel dummies were removed, see Figures 8(c)-B and 11(c), and grooves for the cables of the sensor were cut into the surface by means of an angle grinder. The sensors were installed, see Figure 11(e), whereby the small gaps to the surrounding asphalt were filled with cement paste in order to ensure firm bond, see Figure 11(d). The strain gauges were covered with a sieved asphalt binder course material, followed by manual compaction, see Figures 8(c)-C and 11(f), in order to protect the sensors from damage associated with laydown and compaction.

The following experience was gained with installation method C. Its main advantage is that the dummy place-holders allow for installing the strain gauges at the intended positions, without exposing the real sensors to overly high loads during compaction. Compaction of the asphalt layer into which the sensors are now embedded did not result in

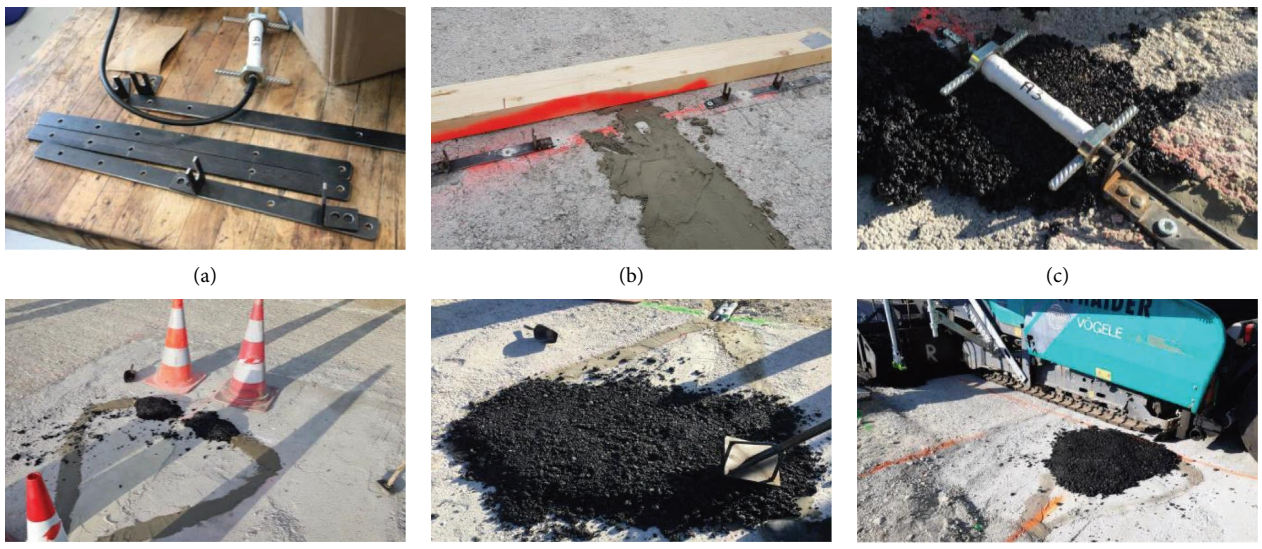

(a) (b) (c)

(d) (e) (f)

Figure 10: Installation of asphalt strain gauges at field-testing site #2 on the A3 using method B: installation in a fixation tool, before asphalt placement.

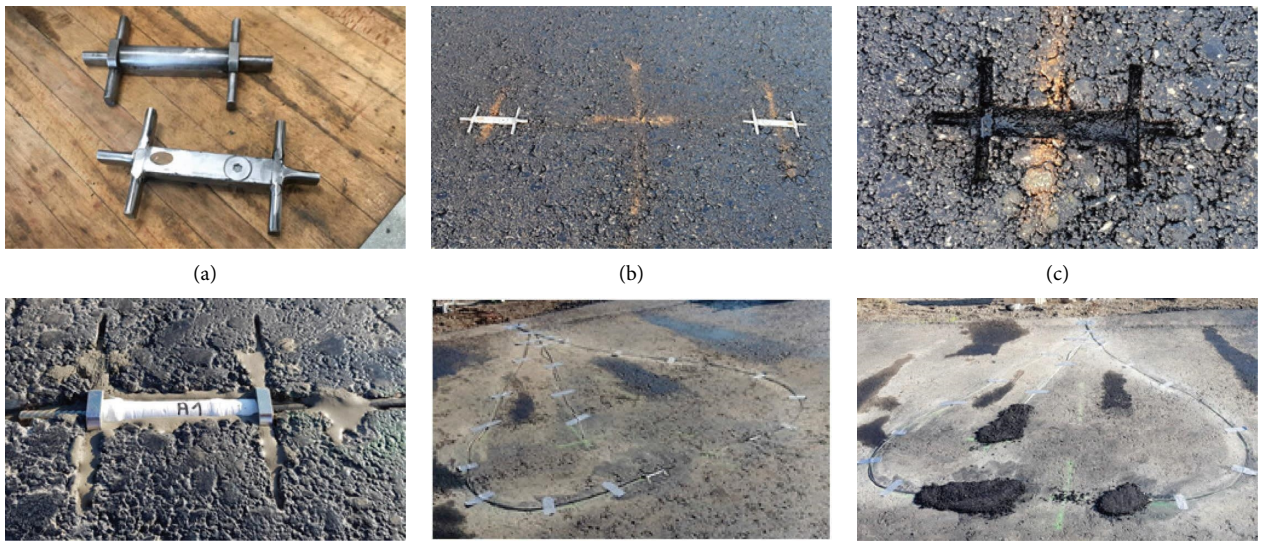

(a) (b) (c)

(d) (e) (f)

Figure 11: Installation of asphalt strain gauges at field-testing site #3 on the S31 using method C: use of steel dummy placeholders for the real sensors.

loading of the sensors because the compaction loads were carried by the dummy place-holders. Compaction of the next asphalt layer on top of the installed sensors did not damage the sensors either because the sensors did not protrude from the surface onto which the next asphalt layer was constructed and because compaction of the new layer resulted in considerable strains in this layer, but not in the much cooler layer underneath, in which the sensors are embedded. The main limitation of this method is that it can only be used, at least in the presented form, for installation of strain gauges at *the top* of an asphalt layer. Both strain gauges installed at field-testing site #3 on the S31 deliver realistic measurements.

5. First Data from Dynamic Testing at the Field-Testing Sites

5.1. Results from Dynamic Field Testing on the Rigid Pavement. Experiments at field-testing site #1 were performed over four days from March 2021 until January 2022. The FWD tests were performed with a maximum force of 200 kN. The number of FWD tests performed immediately one after the other and the corresponding average values of the maximum deflections measured by the geophones and of the maximum strains measured by the asphalt strain gauges are given in Table 5. The deflections measured in September, October, and January are similarly large, while those measured in March are significantly

Table 5: Experimental results from FWD experiments on field-testing site #1: average values (from n_{FWD} tests) of the maximum deflections measured by geophones at different distances from the center of the slab ($w(r)$) and of the maximum tensile strain obtained by the asphalt strain gauges (ε_{ASG}); note that throughout the manuscript, tension is associated with a positive mathematical sign.

		Deflections (mm) measured at a radial distance of:								Strain
Date	n_{FWD}	$r = 0.00$ m	$r = 0.30$ m	$r = 0.60$ m	$r = 0.90$ m	$r = 1.20$ m	$r = 1.50$ m	$r = 1.80$ m	$r = 2.10$ m	ε_{ASG} (-)
Mar 21	23	0.286	0.256	0.225	0.190	0.157	0.124	0.096	0.075	16.6×10^{-6}
Sep 21	15	0.176	0.157	0.135	0.115	0.099	0.081	0.068	0.055	4.9×10^{-6}
Oct 21	17	0.169	0.150	0.131	0.110	0.092	0.075	0.062	0.052	4.6×10^{-6}
Jan 22	12	0.166	0.147	0.129	0.109	0.091	0.076	0.061	0.052	6.6×10^{-6}

Table 6: Experimental results from field-testing site #1: temperature measured at the surface of the slab (T_{surf}), the top and mid-depth of the bottom concrete layer (T_7 and T_6, respectively), the interface between concrete and asphalt (T_5), the interface between asphalt and the cement-stabilized layer (T_4), the interface between the cement-stabilized layer and the unbound layer (T_3), and the interface between the unbound layer and the subgrade (T_2), see also Figure 2.

Date	T_{surf} (°C)	T_7 (°C)	T_6 (°C)	T_5 (°C)	T_4 (°C)	T_3 (°C)	T_2 (°C)
Mar 21	23.4	18.0	12.2	6.6	5.6	5.2	4.7
Sep 21	20.5	19.2	17.3	17.6	18.2	18.9	18.3
Oct 21	10.5	10.5	8.8	9.0	9.6	11.0	12.7
Jan 22	−0.5	−0.6	−0.7	−0.3	0.1	0.7	1.5

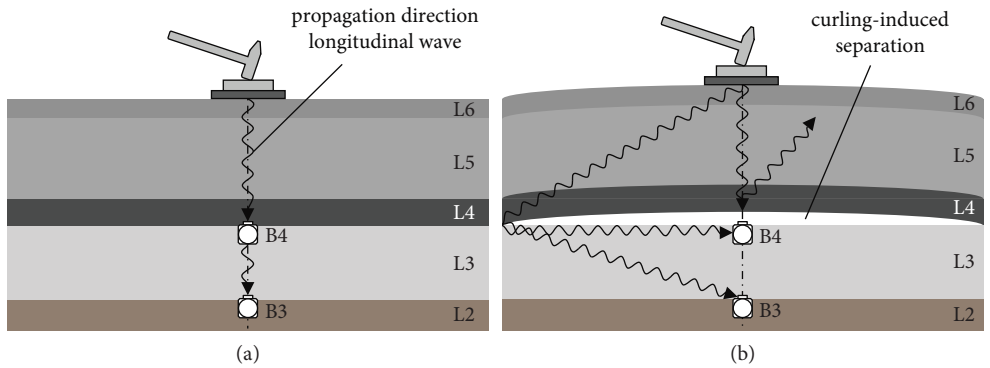

Figure 12: Traveling paths of fronts of elastic waves produced with sledgehammer strokes: (a) situation with full-face contact along all layer interfaces, and (b) situation with slab curling at the center of the slab.

larger. This underlines the challenges associated with the interpretation of FWD test results. Also, the measured asphalt strains underline the outstanding nature of the tests performed in March. The strain measured in spring is equal to 16.6×10^{-6}. This is significantly larger than the strains measured in fall and winter, which range from 4.6×10^{-6} to 6.6×10^{-6}.

The temperatures measured by means of a digital infrared thermometer at the surface of the slab and by means of the Pt100 sensors inside the pavement structure are listed in Table 6. The asphalt temperature amounted to some 6°C in March, some 18°C in September, some 9°C in October, and some 0°C in January, see values of T_5 and T_4 in Table 6. It is concluded that stiffness changes in the asphalt layer must have influenced the behavior of the pavement structure. However, the temperature of asphalt alone cannot explain the significant differences of FWD tests performed in March and in other months (note that the asphalt temperatures were quite similar in March and October). This provides the motivation to discuss, for the results obtained in March, indicators for temperature-induced curling, i.e., for uplift at the center of the slab leading to partial loss of contact along an interface between two adjacent layers of the pavement structure, Figure12(b). This type of slab curling is driven by the temperature difference between the top and the bottom of the slab [94], whereby the top is warmer than the bottom.

The first indicator for slab curling in March is provided by the temperatures measured across the depth of the concrete slab, see T_{surf}, T_7, T_6, and T_5 in Table 6. In January, the temperature of the concrete slab was almost uniform. In March, September, and October, the temperature at the top of the concrete slab was larger than that at its bottom, i.e., $T_{surf} > T_5$. The corresponding temperature difference, T_{surf}-T_5, amounted to 16.8°C in March, 2.9°C in September, 1.5°C in October, and −0.2°C in January, see Table 6. Thus, the temperature gradient experienced by the concrete slab in March was significantly larger than those in other months.

The second indicator for slab curling in March is provided by the measured asphalt strains. In this context, it is recalled that the readings of the strain gauges were set to zero

Table 7: Experimental results from sledgehammer experiments on field-testing site #1: mean values ± standard deviation (from n_{slh} tests) of the time of flight through the cement-stabilized layer (Δt), its wave speed (v_L), and its modulus of elasticity (E), see Table 1 for layer thickness, $h = 17.6$ cm and mass density $\rho = 2568$ kg/m^3, as well as Table 4 for Poisson's ratio $\nu = 0.20$.

Date	n_{slh}	Δt (μs)	v_L (m/s)	E (GPa)
Mar 21	67	⋆	⋆	⋆
Sep 21	49	89.2 ± 7.3	1973 ± 161	9.16 ± 1.24
Oct 21	38	94.2 ± 3.9	1871 ± 77	8.05 ± 0.54
Jan 22	43	98.3 ± 9.7	1809 ± 186	7.70 ± 1.62

⋆Results affected by curling of the concrete slab.

before the first FWD test of the day. In an FWD test on a curling-free pavement, the structure responds to the dynamic loading with the stiffness of a firmly bonded multilayered half-space. This results in tensile strains at the positions of the asphalt strain gauges, as indicated by strains measured during the curling-free FWD tests performed in September, October, and January. An FWD test on a curled pavement structure can be subdivided into two phases. During the first phase, the curled part of the pavement structure is pushed down until full-face contact is reestablished along all interfaces. During the second phase, the pavement structure responds to the continued dynamic loading with the stiffness of a firmly bonded multilayered half-space. Let us consider that loss of contact occurred, in March, in the interface between the asphalt and the cement-stabilized layer, i.e., that the asphalt was well bonded to the concrete slab and curled up together with it. During the first phase of the FWD tests, the sandwich structure consisting of concrete and asphalt layers was pushed from the convexly curved initial configuration down to a plane state. This resulted in a significant tensile strain experienced by the asphalt strain gauges. During the second phase of the FWD tests, the tensile strain increased, similar to the situations in the curling-free FWD tests performed in September, October, and January.

The third indicator for slab curling in March is provided by the results of the sledgehammer tests, see Table 7 for the number of tests performed, corresponding results, and the derived values of the modulus of elasticity of the cement-stabilized layer. The tests performed in September, October, and January delivered stiffness moduli in the overlapping intervals from 9.16 GPa ± 1.24 GPa to 7.70 GPa ± 1.62 GPa. The accelerometer readings recorded in March, in turn, could not be evaluated because the signal arrived at both acceleration sensors virtually at the same time, see Figure 13(a). In addition, the amplitude of the signals captured in March was one order of magnitude smaller than the other months, compare Figures 13(a) and 13(c). These results can be explained as follows.

The sledgehammer strokes were not strong enough to close the curling-induced gap between the asphalt and the cement-stabilized layer. The front of the longitudinal wave propagating vertically downwards was reflected at the upper free surface of the separated interface. Therefore, it did not arrive at the accelerometers below. The wave resulting in the first signals of the accelerometers had to travel *around* the separated interface. This wave was initially traveling diagonally downwards, away from the vertical axis through the accelerometers, towards the edge between the separated region and the contact region of the interface. There, the wave had to change direction and continued to propagate diagonally downwards, but this time underneath the separated region and towards the accelerometers, see Figure 12. The effective propagation distances from the hit surface around the separated interface to the two accelerometers were similarly large. This explains why the wavefront arrived virtually at the same time at the two accelerometers, although they are buried at different depths. The change of the traveling direction of the wavefront at the edge of the separated region, in turn, explains why the recorded accelerations were much smaller in March than that of the curling-free cases of other months.

It is very likely that full-face contact prevailed along all layer interfaces in September, October, and January. Thus, the dynamic wave created by sledgehammer strokes propagated vertically downwards, reaching accelerometer B4 first and accelerometer B3 by some 95 μs later, see Table 7. The difference between the wave arrival times at B4 and B3 could be measured in a straightforward fashion, see Figure 13(c). The accuracy of the results is underlined by the standard deviations of the time of flight, ranging from 4 to 10 μs, see Table 7. This interval is virtually one-to two-times the resolution of the accelerometer readings which were captured with a data acquisition rate of 200 kHz, i.e., every 5 μs.

The accelerometer readings captured during FWD testing, in turn, do not allow for reliable determination of the time of flight through the cement-stabilized layer, see Figures 13(b) and 13(d). The reason will be explained in the next subsection where accelerometer readings are available at four rather than two different depths.

5.2. Results from Dynamic Field Testing on a Flexible Pavement. Experiments at measurement point MP2 of field-testing site #2 were performed over two days in July 2021 and April 2022, respectively. The FWD tests were performed with a maximum force of 150 kN. The number of FWD tests performed immediately one after other, and the corresponding average values of the maximum deflections measured by the geophones are given in Table 8. The strain gauges did not yield readings because they were damaged during installation. The deflections measured in July and April, respectively, are the same (=0.062 mm) in a distance of 2.1 m from the center of the falling weight. This indicates that the subgrade and the bottommost layers of the pavement

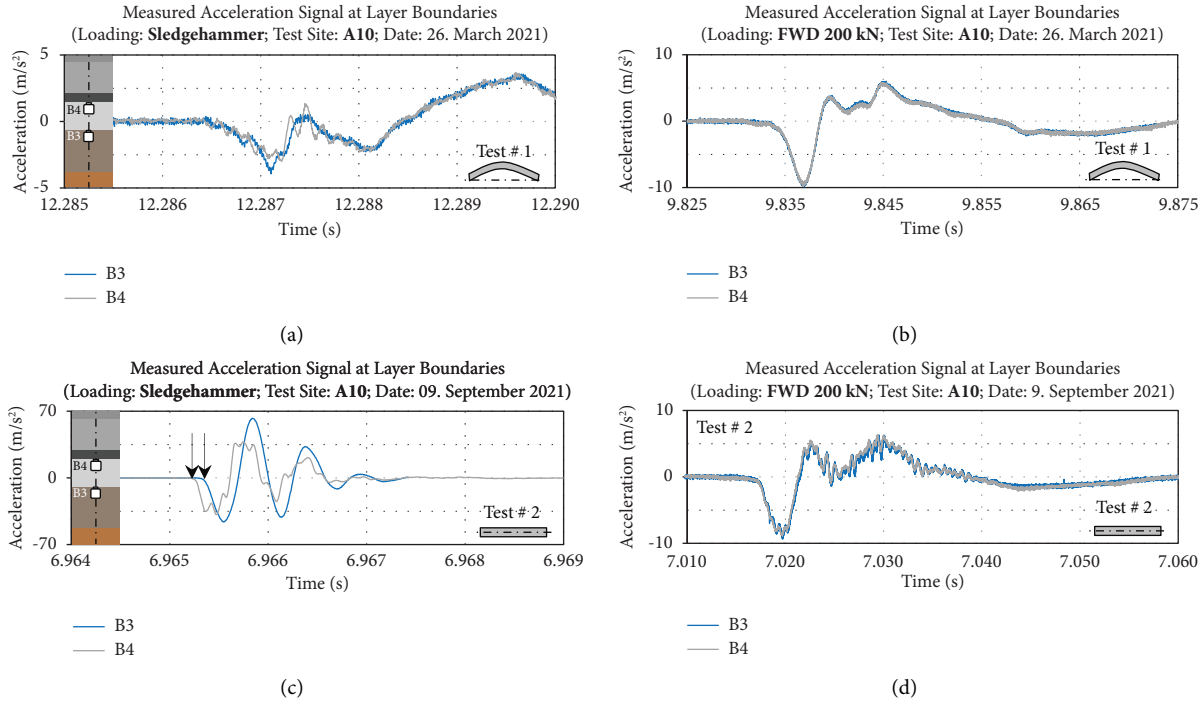

Figure 13: Accelerometer readings from dynamic experiments at field-testing site #1 on the A10: (a, b) showing readings from March 2021 when slab curling occurred; (c, d) showing readings from September 2021 when full-face contact prevailed at all layer interfaces; (a) and (c) show results from sledgehammer tests; (b) and (d) show results from FWD tests.

Table 8: Experimental results from FWD experiments on field-testing site #2: average values (from n_{FWD} tests) of the maximum deflections measured by geophones at different distances from the center of the slab ($w(r)$).

		Deflections (mm) measured at a radial distance of:							
Date	n_{FWD}	$r = 0.00$ m	$r = 0.30$ m	$r = 0.60$ m	$r = 0.90$ m	$r = 1.20$ m	$r = 1.50$ m	$r = 1.80$ m	$r = 2.10$ m
Jul 21	5	0.458	0.239	0.205	0.176	0.140	0.103	0.078	0.062
Apr 22	13	0.256	0.200	0.170	0.145	0.121	0.097	0.076	0.062

Table 9: Experimental results from measurement point MP2 of field-testing site #2: temperature measured at the surface of the slab (T_{surf}), the interface between surface and binder courses (T_6), between binder and base courses (T_5), binder course and lean concrete (T_4), lean concrete and unbound layer (T_3), as well as between unbound layer und subgrade (T_2), see Figure 3.

Date	T_{surf} (°C)	T_6 (°C)	T_5 (°C)	T_4 (°C)	T_3 (°C)	T_2 (°C)
Jul 21	48.7	36.8	31.9	31.4	31.5	30.3
Apr 22	18.8	14.3	12.6	13.2	12.6	11.1

structure had the same stiffness. With increasing proximity to the center of the falling weight, however, the differences between deflections measured in July and April increase both in absolute and in relative terms. At the center of the falling weight, the absolute difference is equal to 0.202 mm, and this equal to 79% of the deflection measured in April. This indicates that the stiffness of the topmost layers of the pavement structure were significantly different in July and April.

The temperatures measured by means of a digital infrared thermometer at the surface of the expressway, and by means of the Pt100 sensors inside the pavement structure, are listed in Table 9. Both times, the temperature in the lean concrete layer was virtually constant. The temperature difference across this layer, T_4-T_3, was as small as −0.1°C in July and +0.6°C in April. This underlines that (i) curling of the lean concrete slab is very unlikely, and (ii) the seasonal differences of the measured surface deflections must have a different origin. Averaging the temperatures measured at the top and the bottom of each one of the three asphalt courses, yields 42.8°C (surface course), 34.4°C (binder course), and 31.7°C (base course) in July and 16.6°C (surface course), 13.5°C (binder course), and 12.9°C (base course) in April. The seasonal temperature differences have resulted in significant stiffness changes of all three asphalt layers. This provides the motivation to discuss layer stiffnesses quantified from sledgehammer tests.

The number of sledgehammer tests performed, corresponding results, and the derived values of moduli of elasticity are listed in Table 10. The values of the thickness, the mass density, and Poisson's ratio of the lean concrete and unbound layers were taken from Tables 2 and 4. As for

Table 10: Experimental results from sledgehammer experiments on measurement point MP2 of field-testing site #2: mean values ± standard deviation (from n_{slh} tests) of the time of flight (Δt), the wave speed (v_L), and the modulus of elasticity (E).

Date	Layer	n_{slh}	Δt (μs)	v_L (m/s)	E (GPa)
Jul 21	Asphalt	40	119.6 ± 11.8	1434 ± 136	3.95 ± 1.35
	Lean concrete	40	156.5 ± 2.7	2109 ± 36	8.67 ± 0.30
	Unbound	40	655.8 ± 12.3	503 ± 9	0.39 ± 0.01
Apr 22	Asphalt	47	93.0 ± 35.5	1997 ± 473	8.63 ± 1.97
	Lean concrete	47	151.4 ± 3.7	2181 ± 53	9.28 ± 0.45
	Unbound	47	643.6 ± 18.0	513 ± 14	0.40 ± 0.02

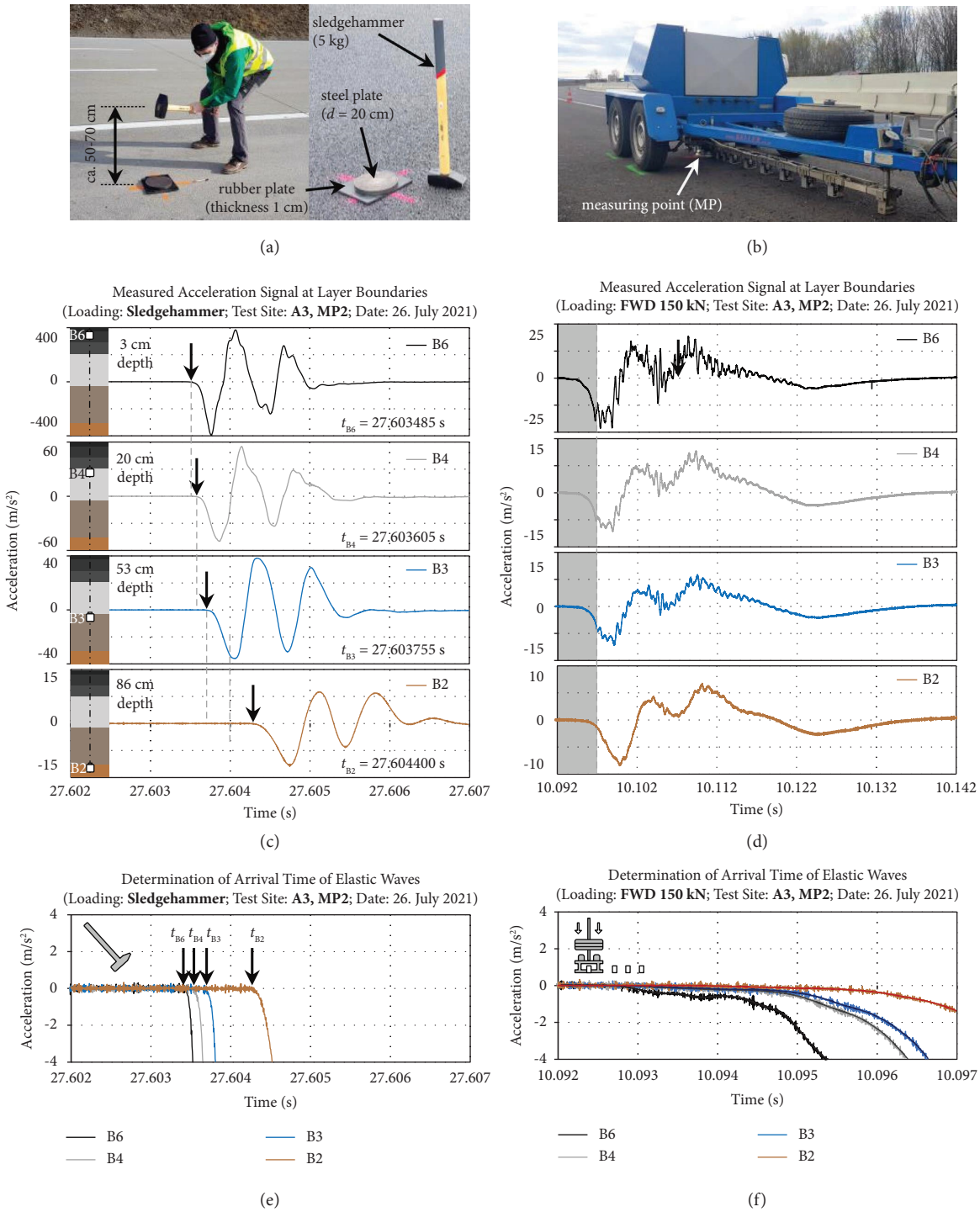

Figure 14: Dynamic experiments at measurement point MP2 of field-testing site #2 on the A3: (a), (c), and (e) refer to sledgehammer tests, (b), (d), and (f) refer to FWD tests: (a, b) showing photos from in situ testing, (c, d) showing the accelerations recorded in one test, (e, f) showing details of the measured accelerations recorded around the arrival of the wave front; the depths of the sensors given in (c) refer to the ones measured in situ.

asphalt, the measured time of flight refers to a sandwich structure consisting of the binder and base courses, see Fig. 3. Its thickness is equal to 17.0 cm, its average mass density to 2,459 kg/m^3, and its Poisson's ratio to 0.3, see Tables 2 and 4.

The seasonal difference in stiffness of the sandwich asphalt layer is significantly larger than that of the lean and unbound layers. For all three layers, the determined stiffness was smaller in July than in April. It was by 54% smaller for the sandwich asphalt layer, by 6.6% smaller for the lean concrete layer, and by 2.5% smaller for the unbound layer.

Both in July and in April, the accelerometer readings from sledgehammer tests could be evaluated in a straightforward fashion, in order to compute times of flight, see Figure 14(c), while the determination of the time of flight was impossible based on the accelerometer readings from FWD tests, see Figure 14(d). This can be explained as follows. The maximum force of the falling weight is much larger than that of the sledgehammer tests. In order to ensure that the pavement structure is not damaged during dynamic testing, the impact of the falling weight must be damped much more than that of the sledgehammer. The wave front of a sledgehammer test is, therefore, much sharper than that of an FWD test, compare Figures 14(e) and 14(f).

When comparing the accelerations recorded during the sledgehammer and FWD tests, see Figures 14(c) and 14(d), the following additional points appear to be interesting:

(1) The peak accelerations produced by the sledgehammer test near the surface are much larger than those obtained during FWD tests, but decrease much more rapidly with increasing depth. In the exemplary sledgehammer test of Figure 14(c), peak accelerations recorded by the sensor closest to the surface and by the deepest sensor amounted to some $\pm 400\,\text{m/s}^2$ and some $\pm 10\,\text{m/s}^2$, respectively. In the exemplary FWD test of Figure 14(d), in turn, the same sensors recorded peak accelerations of some $\pm 20\,\text{m/s}^2$ and $\pm 8\,\text{m/s}^2$.

(2) The waves caused by the sledgehammer had a base-frequency of 1 kHz to 2 kHz. This is by two orders of magnitude larger than the base-frequency of the waves caused by the falling weight. It ranges from 0.01 kHz to 0.03 kHz. Note the different scales of the abscissas of Figures 14(c) and 14(d).

It is concluded that sledgehammer tests are significantly better suited for determination of layer stiffness, based on measured times of flight and the theory of elastic wave propagation through isotropic media. Since sledgehammer tests are not standardized, the testing conditions and the reproducibility of the results are discussed next. The mass of the hammer and the dimensions of both the steel plate and the rubber pad are given in Figure 14(a). The hammer is swung from a vertical distance of approximately 50–70 cm above the road surface without exerting significant extra force so that the hammer falls primary under its own weight. The metal-on-metal impact creates a dynamic excitation with a sharp wave front. The stiff rubber pad ensures full-face contact to the cleaned pavement surface and prevents the latter from being damaged. The height of fall of the hammer is optimized in an iterative fashion by the operator, until acceleration signals are obtained which can be reliably measured by the buried sensors. Given that the tests can be repeated within seconds, this initial optimization takes a few minutes only. In general applications, the optimal height of fall will depend on the damping properties of both the rubber pad and the pavement layers, as well as the depth at which the sensors are installed. The essential feature is the creation of a *sharp* wave front because this is needed for reliable quantification of the time of flight through the layer of interest. Regarding the tests which were carried out at the described testing site, signals with suitably sharp wave fronts could be reproduced very simply in a highly satisfactory fashion. The limiting factor for the evaluation quality is, therefore, rather related to the sensors. An even higher data acquisition rate would have further increased the quality with which the time of flight, the wave speed, and the stiffness of the cement-stabilized layer could be quantified.

6. Conclusions and Future Outlook

One rigid and two flexible pavement structures were equipped, during their construction, with temperature sensors, accelerometers, and strain gauges. The following conclusions are drawn from the experience gained with the installation of the sensors:

(1) The used Pt100 temperature sensors and IEPE accelerometers are suitable for installation in all types of pavement layers. They particularly withstood high temperatures and compaction forces during the construction of asphalt layers.

(2) Sensor overload during hot-state roller compaction of asphalt layers was the main problem encountered with the strain gauges. In order to avoid such problems, it is recommended to install a steel dummy as a placeholder into hot asphalt layers, immediately *after* their construction and right *before* their compaction, to replace the dummy by the actual sensor right before the installation of the next layer, and to fill small gaps between the sensor and the asphalt by cement paste.

The following conclusions are drawn from results of newly proposed sledgehammer tests and FWD experiments performed at the three field-testing sites:

(1) Strokes with a sledgehammer onto a metal plate, transmitted to the pavement structure via a rubber pad, are well suited for quantification of the time of flight of elastic waves through asphalt, cement-stabilized, and unbound aggregate layers, as long as the individual layers directly underneath the hit surface position are in full-face contact. In such cases, stiffness quantification of individual layers is possible using the theory of propagation of elastic longitudinal waves through isotropic media.

(2) Regarding rigid pavements, sledgehammer tests are capable of detecting curling-induced partial loss of contact of concrete slabs from lower layers by which

they are supported. Loss of layer-to-layer contact underneath the falling weight significantly increases measured deflections during FWD testing.

(3) Regarding flexible pavements, seasonal variations of FWD results can be primarily traced back to temperature-induced stiffness variations of asphalt layers. The other unbound and bound layers were found to exhibit significantly smaller stiffness variations.

These conclusions provide motivation for the following future studies:

(1) Data from field testing together with results from laboratory characterization of the stiffness of bound layers of pavement structures will provide a valuable database for the assessment of software which is designed to back-calculate layer stiffness from deflections measured during FWD tests.

(2) Performing sledgehammer tests and FWD experiments repeatedly at the first field-testing site, during the morning of a day with significant solar heating of the surface of the concrete slab, will allow for studying the evolution of slab curling and its influence on surface deflections measured during FWD testing.

(3) Large-scale application of the proposed approaches to real-time pavement monitoring will provide valuable information for the assessment of pavement performance and the optimization of maintenance strategies. Currently, the biggest challenges for such applications are the development of robust low-cost wireless sensors with autonomous energy supply. The proposed approaches for quantification of the stiffness of individual layers will be particularly valuable when used in combination with this sensor technology in the future.

Data Availability

The experimental data used to support the findings of this study are available from the corresponding author upon reasonable request.

Conflicts of Interest

The authors declare that they have no conflicts of interest.

Acknowledgments

The authors thank Mehdi Aminbaghai, Stefan Hofbauer, Wolfgang Dörner, Dominic Hassan, Constantin Kreil, and Michael Haminger (TU Wien, Austria) for their help during the instrumentation of the field-testing sites. Michael Celadnik and Harald Aigner (Nievelt Labor GmbH, Austria) are also acknowledged for conducting FWD measurements and interesting discussion. This research received financial support from the Österreichische Forschungsförderungsgesellschaft (FFG, Austrian Research Promotion Agency) within the BRIDGE-project "Grundlegende Analyse von FWD-Versuchen: Innovative Experimente, moderne Struktursimulationen, statistische Datenanalyse—FALLINGweight." The authors are grateful to the Austrian motorway and expressway operator ASFINAG for the support regarding the selection and instrumentation of the field-testing sites as well as for providing traffic control during in situ measurements. Financial support through the open access funding programme of TU Wien's University Library is also gratefully acknowledged.

References

[1] F. Olard and H. Di Benedetto, "General "2S2P1D" model and relation between the linear viscoelastic behaviours of bituminous binders and mixes," *Road Materials and Pavement Design*, vol. 4, no. 2, pp. 185–224, 2003.

[2] F. Khabaz and R. Khare, "Molecular simulations of asphalt rheology: application of time–temperature superposition principle," *Journal of Rheology*, vol. 62, no. 4, pp. 941–954, 2018.

[3] L. Khazanovich, S. D. Tayabji, and M. I. Darter, "Back-calculation of layer parameters for performance for LTPP test sections," *Volume I: slab on elastic solid and slab on dense-liquid foundation analysis of rigid Pavements*, Tech. Rep. No. FHWA-RD-00-086, United States. Federal Highway Administration. Office of Engineering, McLean, VA, USA, 2001.

[4] J. M. Vandenbossche, *Interpreting falling weight deflectometer results for curled and warped portland cement concrete pavements*, PhD thesis, University of Minnesota, Minneapolis, MN, USA, 2003.

[5] F. Salour and S. Erlingsson, "Moisture-sensitive and stress-dependent behavior of unbound pavement materials from in situ falling weight deflectometer tests," *Transportation Research Record*, vol. 2335, no. 1, pp. 121–129, 2013.

[6] A. Bayat, *Field and numerical investigation to determine the impact of environmental and wheel loads on flexible pavement*, PhD thesis, University of Waterloo, Waterloo, UK, 2009.

[7] Cost, "Use of falling weight deflectometers in pavement evaluation Tech. Rep. COST Action 336," in *European Co-operation in the Field of Scientific and Technical Research*, The Netherlands: European Commission, Directorate General Transport, Brussels, The Netherlands, 2 edition, 2005.

[8] K. D. Smith, J. E. Bruinsma, M. J. Wade, K. Chatti, and J. Vandenbossche, *Using Falling Weight Deflectometer Data With Mechanistic-Empirical Design And Analysis*, Tech. Rep. FHWA-HRT-16-009, United States. Federal Highway Administration, McLean, VA, USA, 2017.

[9] M. Hons, R. Stewart, D. Lawton, M. Bertram, and G. Hauer, "Accelerometer vs. Geophone Response: A Field Case History," in *70th EAGE Conference and Exhibition incorporating SPE EUROPEC 2008*, Citeseer, Calgary, UK, 2008.

[10] R. Brincker, B. Bolton, and A. Brandt, "Calibration and Processing of Geophone Signals for Structural Vibration Measurements," in *Structural Dynamics*, pp. 1375–1379, Springer, 2011.

[11] E. Wielandt, "Seismic sensors and their calibration," in *Deutsches GeoForschungsZentrum GFZ*, pp. 1–51, University of Stuttgart, Stuttgart Germany, 2012.

[12] A. Hossain and J. P. Zaniewski, *Characterization of Falling Weight Deflectometer Deflection basin*, Transportation Research Record, Oaks, CA, USA, 1991.

[13] B. Xu, S. R. Ranjithan, and Y. R. Kim, "New relationships between falling weight deflectometer deflections and asphalt pavement layer condition indicators," *Transportation Research Record*, vol. 1806, no. 1, pp. 48–56, 2002.

[14] G. R. Rada, S. Nazarian, B. A. Visintine, R. V. Siddharthan, and S. Thyagarajan, "Pavement structural evaluation at the network level," Tech. Rep. FHWA-HRT-15-074, United States. Federal Highway Administration. Office of Infrastructure, Washington, DC, USA, 2016.

[15] M. F. Rabbi and D. Mishra, "Using FWD deflection basin parameters for network-level assessment of flexible pavements," *International Journal of Pavement Engineering*, vol. 22, no. 2, pp. 147–161, 2021.

[16] M. S. Hoffman and M. Thompson, *Mechanistic Interpretation of Nondestructive Pavement Testing Deflections*, PhD Thesis, University of Illinois at Urbana-Champaign, Urbana, IL, USA, 1980.

[17] R. Díaz Flores, M. Aminbaghai, L. Eberhardsteiner, R. Blab, M. Buchta, and B. L. Pichler, "Multi-directional Falling Weight Deflectometer (FWD) testing and quantification of the effective modulus of subgrade reaction for concrete roads," *International Journal of Pavement Engineering*, vol. 24, pp. 1–19, 2021.

[18] R. Díaz Flores, M. Aminbaghai, L. Eberhardsteiner, R. Blab, M. Buchta, and B. L. Pichler, "T-shaped arrangement of geophones for rapid quantification of asymmetric behaviour of concrete slabs in central FWD tests," *International Journal of Pavement Engineering*, vol. 24, no. 1, 2023.

[19] R. Díaz Flores, M. Aminbaghai, B. Pichler, L. Eberhardsteiner, R. Blab, and M. Buchta, "Star-shaped Falling Weight Deflectometer (FWD) testing and quantification of the distribution of the modulus of subgrade reaction," in *Computational Modelling of Concrete and Concrete Structures*, pp. 284–293, CRCPress, Boca Raton, FL, USA, 2022.

[20] D. M. Burmister, "The general theory of stresses and displacements in layered systems. I," *Journal of Applied Physics*, vol. 16, no. 2, pp. 89–94, 1945.

[21] R. C. Romeo, R. B. Davis, H. S. Lee, S. A. Durham, and S. S. Kim, "A tandem trust-region optimization approach for ill-posed falling weight deflectometer backcalculation," *Computers & Structures*, vol. 275, Article ID 106935, 2023.

[22] R. Tarefder and M. Ahmed, "Consistency and accuracy of selected FWD backcalculation software for computing layer modulus of airport pavements," *International Journal of Geotechnical Engineering*, vol. 7, no. 1, pp. 21–35, 2013.

[23] H. M. Westergaard, "Stresses in concrete pavements computed by theoretical analysis," *Public Roads*, vol. 7, no. 2, pp. 25–35, 1926.

[24] H. Westergaard, "New formulas for stresses in concrete pavements of airfields," *Transactions of the American Society of Civil Engineers*, vol. 113, no. 1, pp. 425–439, 1948.

[25] A. Ioannides, E. Barenberg, and J. Lary, "Interpretation of falling weight deflectometer results using principles of dimensional analysis," in *Proceedings of the 4th International Conference on Concrete Pavement Design and Rehabilitation*, pp. 231–247, Purdue University, West Lafeyette, IN, USA, April 1989.

[26] A. M. Ioannides, "Dimensional analysis in NDT rigid pavement evaluation," *Journal of Transportation Engineering*, vol. 116, no. 1, pp. 23–36, 1990.

[27] K. T. Hall, M. Darter, T. Hoerner, and L. Khazanovich, "Ltpp data analysis," *Phase i: validation of guidelines for k-value selection and concrete pavement performance prediction*, Tech. Rep. No. FHWA-RD-96-198, Federal Highway Administration, McLean, VA, USA, 1997.

[28] S. M. Zaghloul, *Non-linear Dynamic Analysis of Flexible and Rigid Pavements*, PhD Thesis, Purdue University, West Lafayette, IN, USA, 1993.

[29] M. Li, *Pavement Response Analysis and Modulus Back-Calculation for Highway and Airfield Flexible Pavements*, PhD Thesis, Rutgers University-School of Graduate Studies, New Brunswick, NJ, USA, 2017.

[30] O. C. Assogba, Y. Tan, X. Zhou, C. Zhang, and J. N. Anato, "Numerical investigation of the mechanical response of semi-rigid base asphalt pavement under traffic load and nonlinear temperature gradient effect," *Construction and Building Materials*, vol. 235, Article ID 117406, 2020.

[31] O. C. Assogba, Y. Tan, Z. Sun, N. Lushinga, and Z. Bin, "Effect of vehicle speed and overload on dynamic response of semi-rigid base asphalt pavement," *Road Materials and Pavement Design*, vol. 22, no. 3, pp. 572–602, 2021.

[32] G. Fu, H. Wang, Y. Zhao, Z. Yu, and Q. Li, "Non-destructive evaluation of longitudinal cracking in semi-rigid asphalt pavements using FWD deflection data," *Structural Control and Health Monitoring*, vol. 29, no. 10, p. 3050, 2022.

[33] M. Barriera, S. Pouget, B. Lebental, and J. Van Rompu, "In situ pavement monitoring: a review," *Infrastructure*, vol. 5, no. 2, p. 18, 2020.

[34] T. L. Weinmann, A. E. Lewis, and S. Tayabji, "Pavement sensors used at accelerated pavement test facilities," in *Proceedings of the Second International Conference on Accelerated Pavement Testing*, Saint Paul, MN, USA, January 2004.

[35] M. R. Islam and R. A. Tarefder, "Field measurement of vertical strain in asphalt concrete," *International Journal of Scientific Engineering and Research*, vol. 4, no. 2, pp. 1–6, 2013.

[36] P. Kara De Maeijer, G. Luyckx, C. Vuye et al., "Fiber optics sensors in asphalt pavement: state-of-the-art review," *Infrastructure*, vol. 4, no. 2, p. 36, 2019.

[37] S. Joshi and S. M. Harle, "Linear variable differential transducer (LVDT) & its applications in civil engineering," *International Journal of Transportation Engineering and Technology*, vol. 3, no. 4, pp. 62–66, 2017.

[38] E. Levenberg, "Inferring pavement properties using an embedded accelerometer," *International Journal of Transportation Science and Technology*, vol. 1, no. 3, pp. 229–246, 2012.

[39] C. Sangiorgi, C. Settimi, P. Tataranni, C. Lantieri, and S. Adomako, "Thermal analysis of asphalt concrete pavements heated with amorphous metal technology," *Advances in Materials Science and Engineering*, vol. 2018, Article ID 6382874, 8 pages, 2018.

[40] F. Salour, *Moisture Influence on Structural Behaviour of Pavements: Field And Laboratory Investigations*, PhD Thesis, KTH Royal Institute of Technology, Stockholm, Sweden, 2015.

[41] I. L. Al-Qadi, A. Loulizi, M. Elseifi, and S. Lahouar, "The Virginia Smart Road: the impact of pavement instrumentation on understanding pavement performance," *Journal of the Association of Asphalt Paving Technologists*, vol. 73, no. 3, pp. 427–465, 2004.

[42] X. Tang, S. M. Stoffels, and A. M. Palomino, "Evaluation of pavement layer moduli using instrumentation measurements," *International Journal of Pavement Research and Technology*, vol. 6, no. 6, p. 755, 2013.

[43] H. Cheng, L. Liu, and L. Sun, "Bridging the gap between laboratory and field moduli of asphalt layer for pavement design and assessment: a comprehensive loading frequency-

based approach," *Frontiers of Structural and Civil Engineering*, vol. 16, no. 3, pp. 267–280, 2022.

[44] D. H. Chen, J. Bilyeu, and F. Hugo, "Monitoring pavement response and performance using in-situ instrumentation," *Field Instrumentation for Soil and Rock*, vol. 1358, pp. 121–214, 1999.

[45] N. Tabatabaee and P. Sebaaly, "State-of-the-art pavement instrumentation," *Transportation Research Record*, vol. 1260, pp. 246–255, 1990.

[46] P. Solanki, M. Zaman, K. K. Muraleetharan, and D. Timm, "Evaluation of resilient moduli of pavement layers at an instrumented section on I-35 in Oklahoma," *Road Materials and Pavement Design*, vol. 10, no. 1, pp. 167–188, 2009.

[47] H. Yin, "Simulation of flexible pavement response to FWD loads: a mechanistic approach," *International Journal of Pavement Research & Technology*, vol. 5, no. 4, pp. 257–266, 2012.

[48] A. Mateos, J. P. Ayuso, and B. C. Jáuregui, "Evaluation of structural response of cracked pavements at CEDEX transport research center test track," *Transportation Research Record*, vol. 2367, no. 1, pp. 84–94, 2013.

[49] C. A. Lenngren, "Relating deflection data to pavement strain," *Transportation Research Record*, vol. 1293, pp. 103–111, 1991.

[50] M. H. Shafiee, L. Hashemian, A. Rostami, A. Bayat, and N. Tabatabaee, "Field measurement and modeling of vertical and longitudinal strains from falling weight deflectometer testing," *Journal of Transportation Engineering, Part B: Pavements*, vol. 144, no. 1, Article ID 4017021, 2018.

[51] M. Barriera, J. V. Rompu, J. Blanc, E. Chailleux, B. Lebental, and S. Pouget, "Assessing and predicting fatigue damage of road pavement using embedded sensors and deflection measurements: a full scale test," *Road Materials and Pavement Design*, vol. 22, no. 1, pp. 444–461, 2021.

[52] W. Liu, H. Wang, Z. Zhou, X. Xing, D. Cao, and Z. Jiang, "Optical fiber-based sensors with flexible encapsulation for pavement behavior monitoring," *Structural Control and Health Monitoring*, vol. 22, no. 2, pp. 301–313, 2015.

[53] P. Donovan and E. Tutumluer, "Falling weight deflectometer testing to determine relative damage in asphalt pavement unbound aggregate layers," *Transportation Research Record*, vol. 2104, no. 1, pp. 12–23, 2009.

[54] Z. H. Khan, R. A. Tarefder, and M. A. Hasan, "Field characterization of pavement materials using falling weight deflectometer and sensor data from an instrumented pavement section," *Transportation Research Record*, vol. 2674, no. 4, pp. 205–221, 2020.

[55] R. Bajwa, E. Coleri, R. Rajagopal, P. Varaiya, and C. Flores, "Pavement performance assessment using a cost-effective wireless accelerometer system," *Computer-Aided Civil and Infrastructure Engineering*, vol. 35, no. 9, pp. 1009–1022, 2020.

[56] D. Tompkins, L. Khazanovich, M. I. Darter, and W. Fleischer, "Design and construction of sustainable pavements: Austrian and German two-layer concrete pavements," *Transportation Research Record*, vol. 2098, no. 1, pp. 75–85, 2009.

[57] J. S. Wilson, *Sensor Technology Handbook*, Elsevier, Burlington, MA, USA, 1 edition, 2004.

[58] F. Levinzon, *Piezoelectric Accelerometers with Integral Electronics*, Springer, Cham, Switzerland, 2015.

[59] C. W. De Silva, F. Khoshnoud, M. Li, and S. K. Halgamuge, *Mechatronics: Fundamentals and Applications*, CRC Press, Boca Raton, FL, USA, 2015.

[60] J. Nielsen, E. Levenberg, and A. Skar, "Inference of pavement properties with roadside accelerometers," in *Proceedings of the 9th International Conference on Maintenance and Rehabilitation of Pavements—Mairepav9*, pp. 719–728, Springer, Cham, Switzerland, June 2020.

[61] A. Bohn, P. Ullidtz, R. Stubstad, and A. Sorensen, "Danish experiments with the French falling weight deflectometer," in *Proceedings of the Third International Conference on the Structural Design of Asphalt Pavements*, vol. 1, London, UK, September 1972.

[62] M. Arraigada, M. N. Partl, and S. Angelone, "Determination of road deflections from traffic induced accelerations," *Road Materials and Pavement Design*, vol. 8, no. 3, pp. 399–421, 2007.

[63] T. Ryynänen, T. Pellinen, and J. Belt, "The use of accelerometers in the pavement performance monitoring and analysis," *IOP Conference Series: Materials Science and Engineering*, vol. 10, Article ID 12110, 2010.

[64] N. Bahrani, J. Blanc, P. Hornych, and F. Menant, "Alternate method of pavement assessment using geophones and accelerometers for measuring the pavement response," *Infrastructure*, vol. 5, no. 3, p. 25, 2020.

[65] S. Nazarian, D. Yuan, and V. Tandon, "Structural field testing of flexible pavement layers with seismic methods for quality control," *Transportation Research Record*, vol. 1654, no. 1, pp. 50–60, 1999.

[66] N. Gucunski and A. Maher, *Evaluation Of Seismic Pavement Analyzer For Pavement Condition Monitoring*, Technical Report FHWANJ-2002-012, Federal Highway Administration, Washington, DC, USA, 2002.

[67] K. Tawfiq, J. Armaghani, and J. Sobanjo, "Rational method for selecting seismic waves for pavement evaluation," *Journal of Transportation Engineering*, vol. 128, no. 6, pp. 550–558, 2002.

[68] N. Rydén, *Surface Wave Testing Of Pavements*, PhD Thesis, Department of Engineering Geology, Lund University, Lund, Sweden, 2004.

[69] J. Kumar and P. G. Rakaraddi, "SASW evaluation of asphaltic and cement concrete pavements using different heights of fall for a spherical mass," *International Journal of Pavement Engineering*, vol. 14, no. 4, pp. 354–363, 2013.

[70] A. du Tertre, A. Serhan Kırlangıç, G. Cascante, and S. L. Tighe, "A non-destructive approach for the predictive master curve of asphalt pavements using ultrasonic and deflection methods," *International Journal of Pavement Engineering*, vol. 23, no. 5, pp. 1540–1551, 2022.

[71] C. Kohlhauser and C. Hellmich, "Ultrasonic contact pulse transmission for elastic wave velocity and stiffness determination: influence of specimen geometry and porosity," *Engineering Structures*, vol. 47, no. 5, pp. 115–133, 2013.

[72] J. Carcione, "Wave Fields in Real Media: Wave Propagation in Anisotropic, Anelastic and Porous Media," *Handbook of Geophysical Exploration-Seismic Exploration*, Elsevier Science Ltd, Amsterdam, Netherlands, 1st edition, 2001.

[73] F. Fedorov, *Theory of elastic waves in crystals*, Plenum Press, New York, NY, USA, 1968.

[74] K. Chatti, M. E. Kutay, N. Lajnef, I. Zaabar, S. Varma, and H. S. Lee, "Enhanced analysis of falling weight deflectometer data for use with mechanistic-empirical flexible pavement design and analysis and recommendations for improvements to falling weight deflectometers," *Technical Report FHWA-HRT-15-063*, Federal Highway Administration, Washington, DC, USA, 2017.

[75] H. Kolsky, *Stress Waves in Solids*, Clarendon Press, Oxford, UK, 1953.

[76] FSV, "RVS 03.08.68: rechnerische Dimensionierung von Asphalstrassen [Mechanistic asphalt pavement design, in German]," *Norm, Österreichische Forschungsgesellschaft*

Strasse-Schiene-Verkehr (FSV), Financial Statement Version, Vienna, Austria, 2018.

[77] S. W. Park and R. L. Lytton, "Effect of stress-dependent modulus and Poisson's ratio on structural responses in thin asphalt pavements," *Journal of Transportation Engineering*, vol. 130, no. 3, pp. 387–394, 2004.

[78] Q. T. Nguyen, H. Di Benedetto, Q. P. Nguyen, T. T. N. Hoang, and V. P. Bui, "Effect of time–temperature, strain level and cyclic loading on the complex Poisson's ratio of asphalt mixtures," *Construction and Building Materials*, vol. 294, Article ID 123564, 2021.

[79] H. Liu and R. Luo, "Development of master curve models complying with linear viscoelastic theory for complex moduli of asphalt mixtures with improved accuracy," *Construction and Building Materials*, vol. 152, pp. 259–268, 2017.

[80] K. Omine, H. Ochiai, N. Yasufuku, and H. Sakka, "Prediction of strength-deformation properties of cement-stabilized soils by nondestructive testing," in *Proceedings of the Second International Symposium on Pre-failure Deformation Characteristics of Geomaterials*, pp. 323–330, Balkema, Rotterdam, The Netherlands, June 1999.

[81] E. Binder, M. Königsberger, R. Díaz Flores, H. A. Mang, C. Hellmich, and B. L. Pichler, "Thermally activated viscoelasticity of cement paste: minute-long creep tests and micromechanical link to molecular properties," *Cement and Concrete Research*, vol. 163, Article ID 107014, 2023.

[82] M. Elseifi, "Analysis of seasonal strain measurements in asphalt materials under accelerated pavement testing and comparing field performance and laboratory measured binder tension properties," *Technical Repor FHWA/LA.09/444*, Louisiana Transportation Research Center, Baton Rouge, LA, USA, 2009.

[83] FDOT, *Instrumentation Of Florida's Accelerated Pavement Testing Facility Technical Report*, Florida Department of Transportation, State Materials Office, Gainesville, FL, USA, 2011.

[84] H. Rizvi, A. Ali, Y. Mehta, A. Francoise, C. Purdy, and A. Nolan, "Instrumentation to evaluate the field performance of composite overlays using accelerated pavement testing," in *Bearing Capacity of Roads, Railways and Airfields*, pp. 645–652, CRC Press, Boca Raton, FL, USA, 2017.

[85] B. Pouteau, K. Berrada, and I. Drouadaine, "Smartvia concept: a 5 years feedback on standalone pavement structure monitoring," in *Proceedings of the 6th Eurasphalt & Eurobitume Congress*, pp. 1–13, EAPA, Prague, Czech Republic, June 2016.

[86] N. S. Duong, J. Blanc, P. Hornych, B. Bouveret, J. Carroget, and Y. Le Feuvre, "Continuous strain monitoring of an instrumented pavement section," *International Journal of Pavement Engineering*, vol. 20, no. 12, pp. 1435–1450, 2019.

[87] S. Chun, K. Kim, J. Greene, and B. Choubane, "Evaluation of interlayer bonding condition on structural response characteristics of asphalt pavement using finite element analysis and full-scale field tests," *Construction and Building Materials*, vol. 96, pp. 307–318, 2015.

[88] H. Cheng, L. Liu, and L. Sun, "Determination of layer modulus master curve for steel deck pavement using field-measured strain data," *Transportation Research Record*, vol. 2673, no. 2, pp. 617–627, 2019.

[89] S. Yang, B. Qi, Z. Cao, S. Zhang, H. Cheng, and R. Yang, "Comparisons between asphalt pavement responses under vehicular loading and FWD loading," *Advances in Materials Science and Engineering*, vol. 2020, Article ID 5269652, 15 pages, 2020.

[90] P. Chenevière, M. Wistuba, and A. G. Dumont, "Full-scale testing of pavement response by use of different types of strain gauges," in *Proceedings of the 7th International Conference on the Bearing Capacity of Roads, Railways and Airfields (BCRRA)*, Trondheim, Norway, June 2005.

[91] Y. Seo and J. H. Lee, "Short-and long-term evaluation of asphalt concrete strain gauge installation methods applied to the KHCTR," *Journal of Transportation Engineering*, vol. 138, no. 6, pp. 690–699, 2012.

[92] M. Smith, *ABAQUS/Standard User's Manual, Version 6.9*, Dassault Systèmes Simulia Corp, Johnston, RI, USA, 2009.

[93] FSV, "RVS 11.06.72: tragfähigkeitsmessungen mit dem Fallgewichtsdeflektometer [Measurement of structural capacity with the Falling Weight Deflectometer, in German]," *Norm, Österreichische Forschungsgesellschaft Strasse-Schiene-Verkehr (FSV)*, Financial Statement Version, Vienna, Austria, 2018.

[94] H. T. Yu, L. Khazanovich, M. I. Darter, and A. Ardani, "Analysis of concrete pavement responses to temperature and wheel loads measured from intrumented slabs," *Transportation Research Record*, vol. 1639, no. 1, pp. 94–101, 1998.